J Biol Inorg Chem (2017) 22:339–365
DOI 10.1007/s00775-016-1431-2

MINIREVIEW

Dioxygen activation by nonheme iron enzymes with the 2-His-1-carboxylate facial triad that generate high-valent oxoiron oxidants

Subhasree Kal[1] · **Lawrence Que**[1]

Received: 25 October 2016 / Accepted: 13 December 2016 / Published online: 10 January 2017

Abstract The 2-His-1-carboxylate facial triad is a widely used scaffold to bind the iron center in mononuclear nonheme iron enzymes for activating dioxygen in a variety of oxidative transformations of metabolic significance. Since the 1990s, over a hundred different iron enzymes have been identified to use this platform. This structural motif consists of two histidines and the side chain carboxylate of an aspartate or a glutamate arranged in a facial array that binds iron(II) at the active site. This triad occupies one face of an iron-centered octahedron and makes the opposite face available for the coordination of O_2 and, in many cases, substrate, allowing the tailoring of the iron-dioxygen chemistry to carry out a plethora of diverse reactions. Activated dioxygen-derived species involved in the enzyme mechanisms include iron(III)-superoxo, iron(III)-peroxo, and high-valent iron(IV)-oxo intermediates. In this article, we highlight the major crystallographic, spectroscopic, and mechanistic advances of the past 20 years that have significantly enhanced our understanding of the mechanisms of O_2 activation and the key roles played by iron-based oxidants.

Keywords Nonheme iron enzymes · 2-His-1-carboxylate facial triad · O_2 activation · α-Ketoglutarate-dependent enzymes · Halogenases · Pterin-dependent hydroxylases · Rieske oxygenases

Abbreviations

L-Aba	L-2-Aminobutyric acid
ACCO	1-Aminocyclopropane-1-carboxylate oxidase
ACV	δ-(L-α-Aminoadipoyl)-L-cysteinyl-D-valine
AIB	(α-Aminoisobutyric acid)
AlkB	Enzymes involved in oxidative DNA and RNA repair
AsqJ	4′-Methoxyviridicatin synthase
AsnO	Asparagine oxygenase
BH_4	6(R)-L-erythro-5,6,7,8-tetrahydrobiopterin
BphC	2,3-Dihydroxybiphenyl 1,2-dioxygenase
BZDO	Benzoate 1,2-dioxygense
BDPP	2,6-Bis[[(S)-2-(diphenylhydroxymethyl)-1-pyrrolidinyl]methyl]pyridine dianion
CarC	Carbapenem synthase
CARDO	Carbazole 1,9a-dioxygenase
CAS	Clavaminate synthase
CloR	3-Dimethylallyl-4-hydroxybenzoate synthase
L-Cpg	L-Cyclopropylglycine
Cur Hal	Halogenase in the biosynthesis of curacin A
CytC2	Substrate carrier protein for CytC3 in the biosynthesis of cytotrienin
CytC3	Halogenase in the biosynthesis of cytotrienin
DAOCS	Deacetoxycephalosporin C synthase
DdaC	Epoxidase in biosynthesis of N_β-epoxysuccinamoyl-DAP-Val
DFT	Density functional theory
DMO	Dicamba O-demethylase
L-DOPA	L-3,4-Dihydroxyphenylalanine
EFE	Ethylene forming enzyme
ENDOR	Electron nuclear double resonance
EPR	Electron paramagnetic resonance
EXAFS	Extended X-ray absorption fine structure
FIH-1	Factor-inhibiting hypoxia-inducible factor-1
FtmOx1	Fumitremorgin B endoperoxidase

Electronic supplementary material The online version of this article (doi:10.1007/s00775-016-1431-2) contains supplementary material, which is available to authorized users.

✉ Lawrence Que
larryque@umn.edu

[1] Department of Chemistry, Center for Metals in Biocatalysis, University of Minnesota, Minneapolis, MN 55455, USA

HEPD	2-Hydroxyethylphosphonate dioxygenase
HMS	4-Hydroxymandelate synthase
1-HPP	1-Hydroxypropylphosphonate
2-HPP	2-Hydroxypropyl-1-phosphonate
HPPD	4-Hydroxyphenylpyruvate dioxygenase
HppE	(*S*)-2-Hydroxypropylphosphonate epoxidase
HYSCORE	Hyperfine sublevel correlation spectroscopy
IPNS	Isopenicillin *N* synthase
α-KG	α-Ketoglutarate
KIE	Kinetic isotope effect
KshAB	3-Ketosteroid 9α-hydroxylase
MCD	Magnetic circular dichroism
NDO	Naphthalene 1,2-dioxygenase
N4Py	*N*,*N*-bis(2-pyridylmethyl)-*N*-bis(2-pyridyl) methylamine
NRVS	Nuclear resonance vibrational spectroscopy
L-Nva	L-Norvaline
OMO	2-Oxoquinoline 8-monooxygenase
OrfP	Enzyme that catalyzes conversion of L-Arg into (3R,4R)-$(OH)_2$-L-Arg
P4H	Prolyl-4-hydroxylase
PenD	Epoxidase in biosynthesis of pentalenolactone
PheH	Phenylalanine hydroxylase
PrnD	Aminopyrrolnitrin oxygenase
RedG	Rieske enzyme that catalyzes the oxidative carbocyclization of undecylprodigiosin to form streptorubin B
RFQ	Rapid-freeze-quench
SIE	Solvent isotope effect
SnoK	Carbocyclase in nogalamycin biosynthesis
SnoN	Epimerase in nogalamycin biosynthesis
Stc2	Stachydrine demethylase
SyrB1	Substrate carrier protein for SyrB2 in syringomycin biosynthesis
SyrB2	Halogenase in syringomycin biosynthesis
TauD	Taurine:α-KG dioxygenase
TDO	Toluene dioxygenase
THA	3-(2-Thienyl)-L-alanine
TMC	1,4,8,11-Tetramethyl-1,4,8,11-tetraazacyclotetradecane
TQA	Tris(quinolyl-2-methyl)amine
TrpH	Tryptophan hydroxylase
TyrH	Tyrosine hydroxylase
WelO5	Halogenase involved in the maturation process to form welwitindolinones
XRD	X-ray diffraction

Introduction

It has been 20 years since the term "2-His-1-carboxylate facial triad" was coined to describe what appeared to be a recurring structural motif in an emerging class of dioxygen activating mononuclear nonheme iron enzymes [1]. At that time, crystal structures of the extradiol cleaving 2,3-dihydroxybiphenyl 1,2-dioxygenase (BphC; PDB ID: 1HAN and 1DHY), the pterin-dependent tyrosine hydroxylase (TyrH; PDB ID: 1TOH), and isopenicillin *N* synthase (IPNS; PDB ID: 1IPS, 1BK0 and 1BLZ) had just been solved, revealing a trio of residues, namely two histidines and one carboxylate, that comprised one face of an octahedral iron active site. Although there was no sequence similarity among these three enzymes, it was clear from sequence information that homologies could be discerned among enzymes within the same class such as the extradiol cleaving catechol dioxygenases and the pterin-dependent aromatic amino acid hydroxylases [2]. On the other hand, even though IPNS carried out a unique reaction [3], sequence homologies could be found with the ethylene forming 1-aminocyclopropane-1-carboxylate oxidase (ACCO) [4] and enzymes that required α-ketoglutarate (α-KG) as a co-substrate [5]. Subsequent structural studies confirmed a 2-His-1-carboxylate facial triad motif for binding the catalytic iron(II) center in the active sites of these enzymes [6], a group that has expanded to include the Rieske oxygenases [7, 8], (*S*)-2-hydroxypropylphosphonate epoxidase (HppE) [9], and 2-hydroxyethylphosphonate dioxygenase (HEPD) [10]. In addition, α-KG-dependent halogenases have been identified as, a subset of the family of α-KG-dependent enzymes in which the carboxylate has been replaced by a halide ion [11]. At this point in time, crystal structures are available for 80 different enzymes belonging to this super-family with 2-His-1-carboxylate facial triad active sites (Table S1). The collective information available demonstrates the versatility of the 2-His-1-carboxylate facial triad as a platform for catalyzing a broad range of metabolically important oxidations.

The occurrence of the 2-His-1-carboxylate facial triad in the active sites of so many different types of nonheme iron(II) enzymes suggests an important mechanistic role for this common structural feature. Besides providing three protein-based ligands to anchor the iron in the active site, the facial triad offers the possibility of three additional sites to bind exogenous ligands such as substrate and O_2 to tune the chemistry at the active site and accommodate a variety of catalytic scenarios. Upon substrate and co-substrate

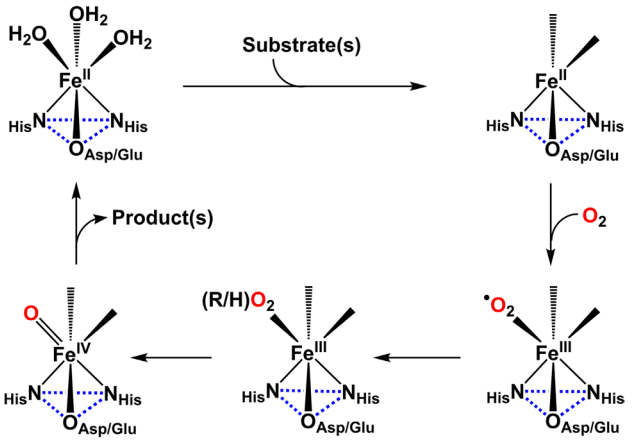

Scheme 1 A general mechanistic scheme for mononuclear nonheme iron enzymes with an active site consisting of a 2-His-1-carboxylate facial triad. The resting enzyme has an iron(II) center that can bind three exogenous ligands, often a bidentate substrate and O_2

binding to the active site, a 5-coordinate iron(II) center is generated that is poised for O_2 activation (Scheme 1). The O_2 adduct, typically described as a superoxoiron(III) species, may react with the substrate or be reduced to a peroxoiron(III) species. Further activation of the latter can generate a high-valent iron species responsible for oxidizing the substrate into product, many examples of which have been trapped and characterized through the pioneering efforts of Krebs and Bollinger [12, 13]. Dioxygen-derived intermediates prior to the cleavage of the O–O bond have also been observed, providing evidence for the superoxo and peroxo intermediates [14–16]. Commensurate with the increase in the number of enzymes using this platform and in the types of reactions catalyzed, status updates on this subject have appeared over the years [2, 14, 17–22]. This review aims to provide a 20-year perspective on this remarkable super-family of enzymes and highlight advances in our understanding of the amazing chemistry that occurs at this rudimentary metal binding motif.

1. α-KG-dependent enzymes

Enzymes that require α-KG as a cosubstrate comprise the largest sub-class in the family of O_2-activating nonheme iron enzymes. They perform a wide variety of transformations including hydroxylation, desaturation, epimerization, heterocyclic ring formation and expansion, epoxidation, and endoperoxide formation as well as halogenation. These enzymes are involved in many important biological processes [23] including O_2 sensing in cells [24], DNA and RNA repair [25], histone demethylation in epigenetic regulation [26], post-translational modification of amino acid side chains in various protein targets [24, 27, 28], and biosynthesis of antibiotics [29]. Their importance in biology has engendered many reviews on this class of enzymes [13, 17, 18, 20]. Scheme 2 shows a sampling of reactions catalyzed by α-KG-dependent enzymes. Scheme 3 presents the consensus mechanism for dioxygen activation associated with this class, which was based on a mechanism proposed for prolyl-4-hydroxylase (P4H) by Hanauske-Abel and Günzler more than three decades ago [30]. In this mechanism, the α-KG co-substrate and the substrate bind sequentially to generate an iron(II) center ready to bind and activate O_2. The bound O_2 carries out a nucleophilic attack on the electrophilic carbonyl group of α-KG, resulting in the loss of CO_2 and the formation of a species that oxidizes the substrate. In this section, we focus on the nature of the O_2-derived iron-based oxidant and its versatile oxidative capabilities.

A. Hydroxylation

The most common reaction catalyzed by α-KG-dependent iron enzymes is the hydroxylation of substrate C–H bonds. This reaction occurs on an asparagine residue of the hypoxia-inducible factor by the FIH-1 enzyme to sense hypoxia in cells, on methyl groups of *N*-methylated nucleotides in DNA and RNA by some members of the family of AlkB enzymes in DNA and RNA repair processes, and on the C2-atom of phytanoyl-CoA by phytanoyl-CoA 2-hydroxylase, to name a few examples. Hydroxylation is performed following the consensus mechanism described in Scheme 3. The high-valent oxoiron(IV) intermediate hydroxylates the target C–H bond by abstracting the H-atom and generating a radical that rebounds to the incipient Fe^{III}–OH (Scheme 3). This mechanism has been validated in recent studies of various α-KG-dependent enzymes [13].

XRD studies on various enzymes in this family have provided snapshots of the iron active site as it proceeds through the catalytic cycle from E to E·α-KG and then to E·α-KG·substrate states (Fig. 1). The iron(II) center in the resting enzyme is bound to a 2-His-1-carboxylate facial triad and three water molecules. Two of these water molecules are displaced upon binding of the bidentate α-KG co-substrate, and the third is lost upon substrate binding in the active site. The substrate does not act as a ligand to the iron but is bound close by such that the target C–H bond points to the empty sixth site where O_2 presumably binds. At this point O_2 activation is initiated and substrate oxidation ensues.

Taurine:α-KG dioxygenase (TauD) catalyzes the hydroxylation of taurine (2-aminoethanesulfonate) (reaction a in Scheme 2) at the carbon next to the sulfonate group to form a hydroxylated product that in turn decomposes to give aminoacetaldehyde and sulfite, as part of Nature's effort to recycle inorganic sulfur. TauD is the first mononuclear nonheme

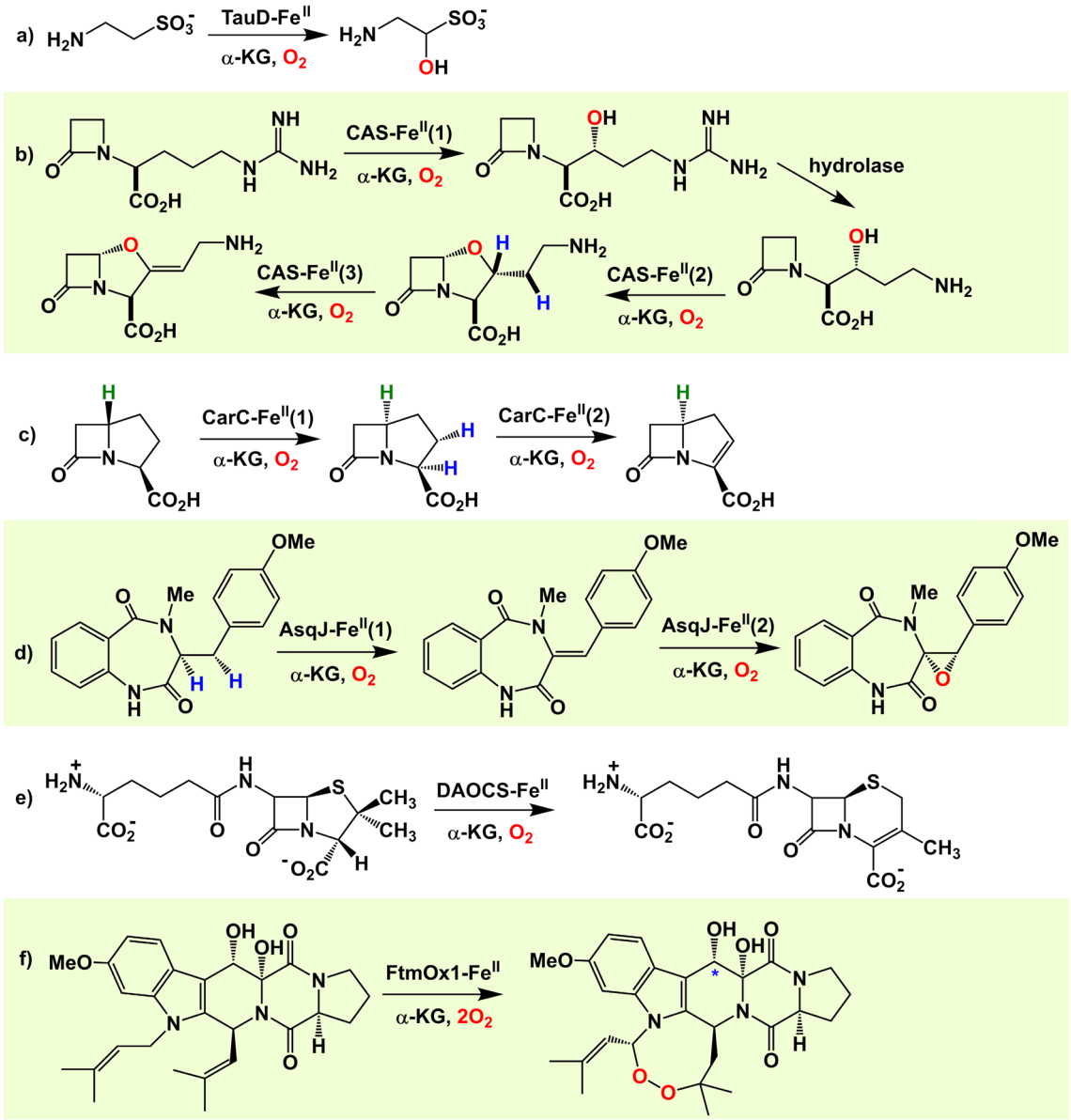

Scheme 2 Select transformations performed by α-KG-dependent enzymes discussed in this section. In all cases there are two other products, succinate and CO_2, which are not shown; they derive from the oxidative decarboxylation of α-KG en route to the generation of the Fe^{IV}=O oxidant. For enzymes that perform multiple reactions, the *numbers in parentheses* indicate their respective places in the reaction sequence. In reaction *f*, the *asterisked* C-atom undergoes further 2-e^--oxidation under experimental reaction conditions

iron enzyme for which an oxoiron(IV) intermediate has been identified by Bollinger and Krebs [31]. O_2 binding to the E·α-KG·taurine complex initiates a cascade of steps that leads to the formation of the high-valent intermediate named TauD-***J***. A rapid-freeze-quenched (RFQ) sample of the intermediate was prepared from the reaction of O_2 with the TauD·α-KG·taurine complex and characterized by Mössbauer spectroscopy to reveal a high-spin ($S = 2$) Fe^{IV} center with an isomer shift (δ) of 0.30 mm s^{-1} and a quadrupole splitting of -0.90 mm s^{-1} [31, 32]. Subsequent efforts by Proshlyakov and Hausinger using continuous flow resonance Raman spectroscopy led to the observation of an ^{18}O-sensitive vibration at 821 cm^{-1} that was assigned to an Fe^{IV}=O unit [33], a result further corroborated in EXAFS studies of Riggs-Gelasco et al. that demonstrate the presence of a short Fe–O distance of 1.62 Å [34]. TauD-***J*** was also shown to be responsible for abstracting the H-atom from the C1 carbon atom of taurine based on the large KIE of ~50 observed for its decay in the presence of C1-deuterio-taurine [32, 35]. A more detailed discussion of various spectroscopic experiments on TauD can be found in another article in this issue by Proshlyakov, McCracken, and Hausinger [36].

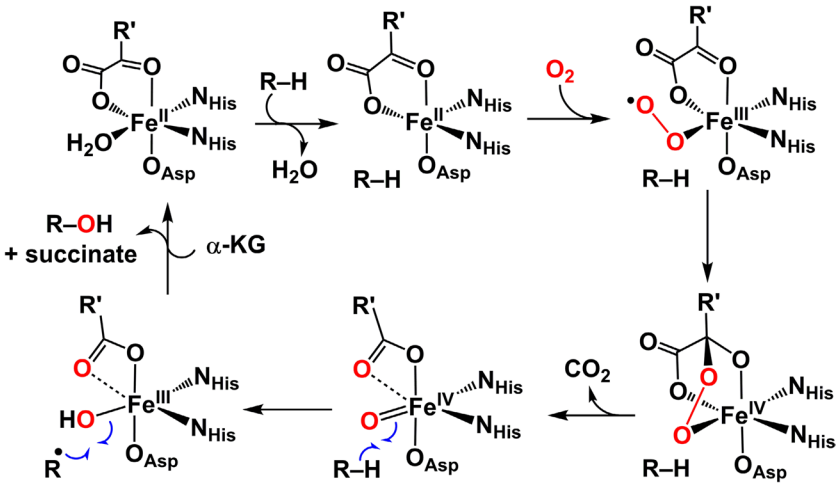

Scheme 3 Consensus mechanism for α-KG-dependent enzymes (illustrating hydroxylation). R′ is the $–CH_2CH_2COO^-$ side chain on the α-KG co-substrate. *Dashed lines* indicate ambiguity in the binding mode of the carboxylate in the succinate byproduct

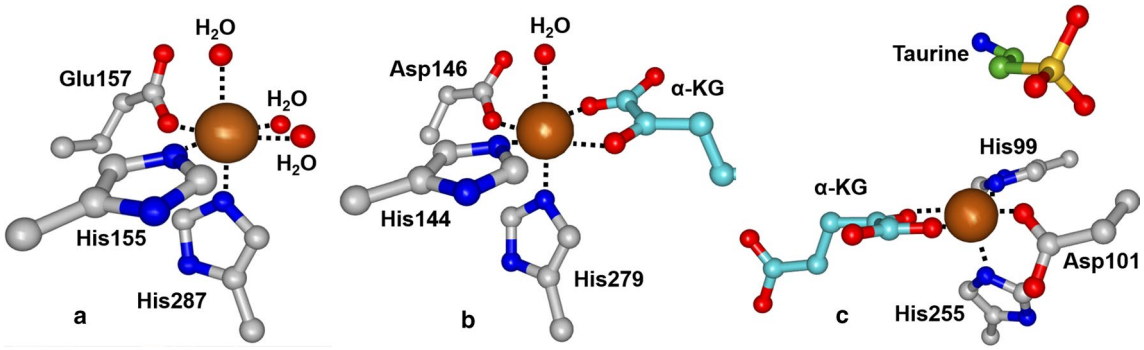

Fig. 1 Snapshots of the iron active site in α-KG-dependent hydroxylases as it proceeds through the catalytic cycle. *Left to right* **a** AsnO, with three bound water molecules (PDB ID: 2OG6); **b** CAS·α-KG complex with one bound water molecule (PDB ID: 1DS1); **c** TauD·α-KG·substrate complex with no bound water molecule (PDB ID: 1GQW). Atom *color code brown* = iron; *blue* = nitrogen; *red* = oxygen; *gray* = enzyme residue carbon; *yellow* = taurine sulfur; *green* = taurine carbon; *light blue* = α-KG carbon

A related Fe^{IV}=O intermediate was trapped for P4H and found to exhibit Mössbauer parameters comparable to TauD-***J*** (Table 1) as well as a ^{2}H-KIE of ~60 for its decay in the presence of protio- and deuterio-substrate [37]. This striking similarity between two enzymes with very different substrates suggests that all α-KG-dependent hydroxylases may share a common mechanism.

Interestingly, OrfP was recently found to catalyze a stereo- and regiospecific double hydroxylation of its L-Arg substrate at its β and γ positions en route to the biosynthesis of the unusual bicyclic amino acid streptolidine, which is a component of the antibiotic streptothricin-F [38]. Crystal structures show the binding of the arginine substrate in a pocket adjacent to the iron center in the OrfP active site as well as its mono- and di-hydroxylated product in the OrfP·product complexes. These results suggest that OrfP may perform two cycles of oxygen activation to carry out the two hydroxylation reactions in sequence, without the monohydroxylated product dissociating from the pocket as the active site recharges for the second hydroxylation. Other enzymes in this class can also catalyze sequential α-KG-dependent transformations at the same active site, as discussed in following sections.

B. Desaturation

There are several examples of α-KG-dependent iron enzymes that catalyze substrate desaturation, namely clavaminate synthase (CAS), carbapenem synthase (CarC), and AsqJ in the biosynthesis of 4′-methoxyviridicatin (reactions b3, c2, and d1, respectively, in Scheme 2). These three enzymes carry out multiple transformations on their respective substrates, requiring the oxidative decarboxylation of an equivalent of α-KG for each step. CAS catalyzes hydroxylation, heterocyclic ring formation, and desaturation (Scheme 2b), CarC carries out epimerization and desaturation (Scheme 2c), and AsqJ performs desaturation and epoxidation (Scheme 2d). A high-spin Fe^{IV}=O oxidant akin to TauD-***J*** is presumed to be formed in these transformations and has been trapped and characterized for CarC and AsqJ.

Table 1 Properties of O_2-derived enzyme intermediates and related model complexes

Enzyme or model complex	Mössbauer parameters δ and [$\lvert\Delta E_Q\rvert$] (mm s^{-1})	Structural data from XRD or *EXAFS*	References
$S = 2$ Fe^{IV}=O			
TauD	0.30 [0.90]	*1.62 Å (Fe–O)*	[32, 34]
AsqJ	0.31 [0.68]		[39]
P4H	0.30 [0.82]		[37]
CarC	0.28 [0.87]		[40]
CytC3-Cl ·L-Aba-CytC2	0.22 [0.70] (0.55)[a] 0.30 [1.09] (0.44)[a]		[41]
CytC3-Br ·L-Aba-CytC2	0.23 [0.81] (0.79)[a] 0.31 [1.06] (0.21)[a]	*1.62 Å (Fe–O)* *2.43 Å (Fe–Br)*	[42]
SyrB2-Cl ·L-Thr-SyrB1	0.23 [0.76] (0.2)[a] 0.30 [1.09] (0.8)[a]	*1.66 Å (Fe–O)* *2.31 Å (Fe–Cl)*	[43]
SyrB2-Cl ·L-Cpg-CytC2	0.25 [0.68] (0.75)[a] 0.29 [1.13] (0.25)[a]		[44]
SyrB2-Br with ·L-Cpg-CytC2	0.25 [0.77] (0.9)[a] 0.29 [1.10] (0.1)[a]		[44]
PheH	0.28 [1.26]		[45]
TyrH	0.25 [1.27]		[46]
IPNS	0.27 [0.44]		[16]
$[Fe^{IV}(O)(TQA)(NCCH_3)]^{2+}$ [b]	0.24 [1.05]		[47]
$[Fe^{IV}(O)(TQA)(Cl)]^{+}$ [b]	0.22 [0.96]		[48]
$[Fe^{IV}(O)(TQA)(Br)]^{+}$ [b]	0.21 [0.94]		[48]
Fe^{III}-peroxo			
BZDO	0.50 [0.5]		[49]
NDO		1.8, 2.0 Å (Fe–η^2 –O_2) (1O7N)	[50]
CARDO		1.8, 1.8 Å (Fe–η^2 –O_2) (3VMI)	[51]
$[Fe^{III}(\eta^2\text{-}O_2)(TMC)]^{+}$	0.58 [0.92]	1.906, 1.914 Å *1.93 Å (Fe–O)*	[52, 53]
$[Fe^{III}(\eta^2\text{-}O_2)(N4Py)]^{+}$	0.61 [1.11]	*1.93 Å (Fe–O)*	[54]
Fe^{III}-superoxo			
IPNS	0.53 [1.02]		[16]
$[Fe^{III}(O_2)(BDPP)]$	0.58 [1.65]	EPR $g_{exc} = 8.03$ $J < 0$; $\lvert J\rvert > 15$ cm^{-1}	[55, 56]

[a] Fractional amounts of the two observed Fe^{IV} species

[b] Although all the enzymatic Fe^{IV}=O intermediates to date have an $S = 2$ spin state, most of the over 70 synthetic Fe^{IV}=O complexes found thus far have an $S = 1$ state [57, 58]. Of the handful of synthetic $S = 2$ Fe^{IV}=O complexes that have been characterized, only the Fe^{IV}(O)(TQA) complexes [47, 48] have Mössbauer isomer shifts that match those of the enzymatic intermediates

However, the mechanistic roles of these Fe^{IV}=O oxidants have only been clarified for the partner reactions, namely the epimerization step of CarC and the epoxidation step for AsqJ, which will be discussed in subsequent sections of this review. From a mechanistic standpoint, substrate hydroxylation and desaturation can be considered to share a common first step, namely the initial H-atom transfer from a substrate C–H bond to the Fe^{IV}=O unit, and then diverge in the following step. For hydroxylation, the nascent carbon radical undergoes rebound with the incipient Fe^{III}–OH moiety to form a C–OH bond, but for desaturation a second H-atom is abstracted from an adjacent C–H bond to form the product C=C bond. Solomon has suggested that these reactivities are modulated by the affinity of water for the iron(II) center in the product complex [59], while Shaik has proposed that the mechanistic switch depends on the ligand sphere flexibility of the oxoiron(IV) species, the nature of the substrate, and the spin states of the reaction pathways [60].

C. Epimerization

Epimerization of a substrate C–H bond is another reaction catalyzed by α-KG-dependent enzymes, as exemplified by CarC in the conversion of (3*S*,5*S*)-carbapenam to

Scheme 4 Proposed epimerization mechanism for CarC

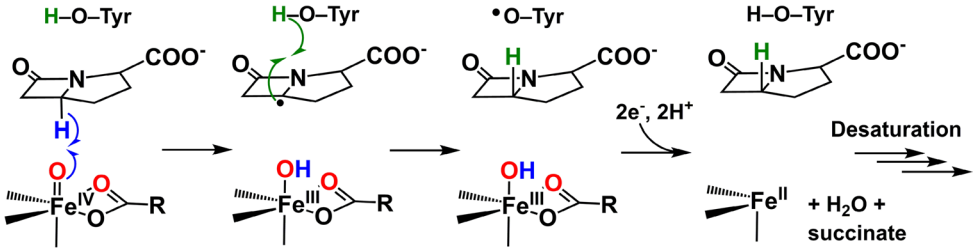

(3*S*,5*R*)-carbapenam (reaction c1 in Scheme 2) and SnoN in the inversion of stereochemistry at the C4″-atom of the precursor of the antibiotic nogalamycin (Scheme 5, reaction b) [61]. As introduced in the previous subsection, CarC performs two steps in the biosynthesis of carbapenam antibiotics; in this subsection we will focus on the epimerization step. The finding that CarC catalyzes a redox-neutral epimerization reaction, rather than an oxidative transformation, raises the mechanistic question of why this transformation would require α-KG and O_2 [62–66]. Insight into this paradoxical situation was obtained from elegant studies by Bollinger, Krebs, and Boal [40]. Mössbauer characterization of an RFQ sample showed the formation of a high-spin ($S = 2$) Fe^{IV}=O intermediate with a quadrupole doublet characteristic of an $S = 2$ Fe^{IV}=O unit (Scheme 4, Table 1). However, upon reaction with substrate, the Fe^{IV}=O intermediate decayed to form a persistent high-spin ($S = 5/2$) Fe^{III} species. This outcome has not been observed for other α-KG-dependent enzymes and suggests that the Fe^{IV}=O intermediate carried out a one-electron oxidation of the substrate. The appearance of the $S = 5/2$ Fe^{III} species was accompanied by the growth of the EPR signal associated with a tyrosyl radical, which was confirmed by stopped-flow optical absorption spectroscopy. Use of the C5-deuterated substrate slowed the decay of the Fe^{IV}=O intermediate, demonstrating that it was responsible for abstracting the C5–H atom. Hence, it was proposed that the Fe^{IV}=O intermediate abstracts the H-atom from C5 of substrate to generate a substrate radical that in turn abstracts an H-atom from a tyrosine residue [40] (Scheme 4).

This mechanistic picture was beautifully corroborated by X-ray crystallography. The crystal structure of the enzyme·α-KG·substrate complex shows the substrate to occupy a position halfway between the iron center and Y165 [40] (Fig. 2). Thus the initial H-atom abstraction by the Fe^{IV}=O unit occurs on one face of the substrate, but the subsequent H-atom transfer from Y165 takes place on the opposite face to ensure formation of the epimeric product. The key role played by Y165 was further confirmed by mutagenesis experiments replacing the tyrosine residue with phenylalanine, which prevented formation of the tyrosyl radical and the epimerized product. In addition, it should be noted that the epimerization reaction is stoichiometric in the absence of a reductant, and additional electrons are required to reduce the Fe^{III} and Y165• to initiate another cycle of dioxygen activation to perform the following desaturation step as well as subsequent turnovers of the overall reaction.

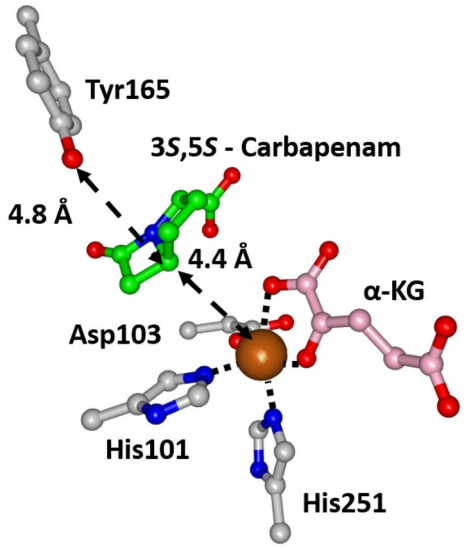

Fig. 2 Active site structure of the CarC·α-KG·substrate complex. (PDB ID: 4OJ8). Atom *color code brown* = iron; *blue* = nitrogen; *red* = oxygen; *gray* = enzyme residue carbon; *green* = carbapenam carbon; *pink* = α-KG carbon

Another α-KG-dependent epimerase SnoN was recently discovered and crystallographically characterized [61] (Scheme 5, reaction b). In the structure of the enzyme·substrate complex, the substrate carbon atom at which epimerization occurs (C4″) was found to be 3.5 Å from the oxygen atom of the water ligand to the iron center, suggesting the likely role of an Fe^{IV}=O moiety as the H-atom abstraction agent. However, mutagenesis studies on the nearby residues did not implicate any of these residues as the H-atom donor, so amino acid side chains might not be involved in the reaction of SnoN. Further experiments are required to identify the possible H-atom donor in this case.

D. Heterocyclic ring formation and expansion

Heterocyclic ring formation and expansion are also transformations related to hydroxylation. Deacetoxycephalosporin

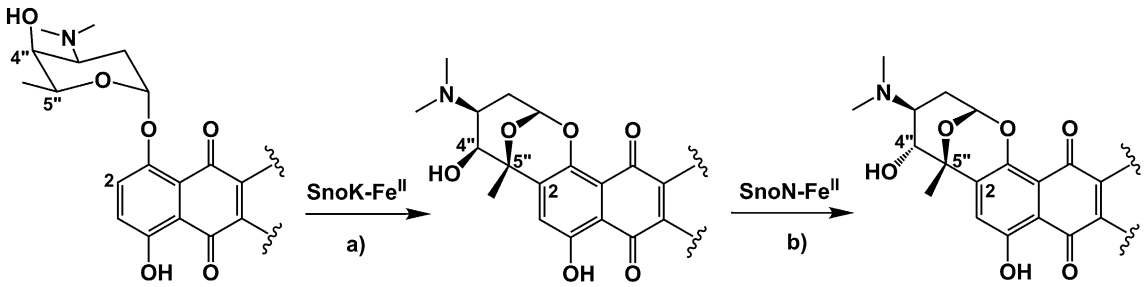

Scheme 5 Reaction scheme for SnoK and SnoN involved in nogalamycin biosynthesis. Only the segment of the substrate structure affected by enzymatic transformations is shown here

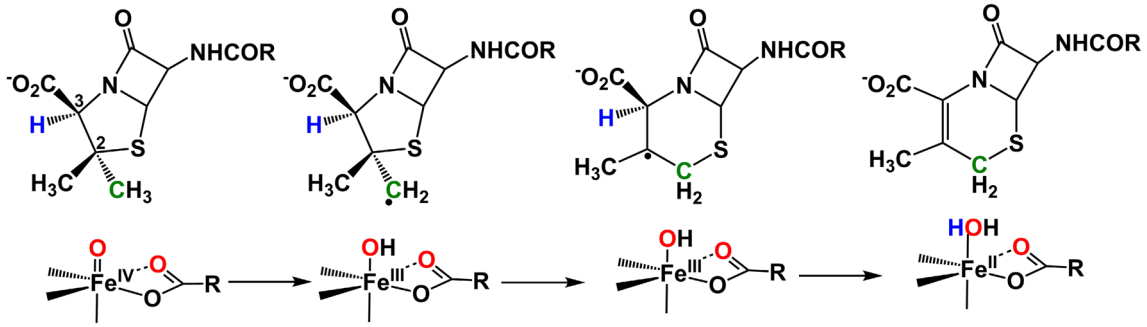

Scheme 6 Proposed ring expansion mechanism initiated by the Fe^{IV}=O intermediate of DAOCS

C synthase (DAOCS) is an example of a ring expansion enzyme; it converts the five-membered thiazolidine ring of penicillin *N* into the six-membered dihydrothiazine ring of cephalosporins (reaction e in Scheme 2) [29, 67]. Exposure of the DAOCS·α-KG·penicillin *N* complex to O_2 elicits a transient species with an absorption band at 310 nm, which decays to form the product complex [68]. By analogy to observations for TauD and P4H [31, 37], this transient species would likely be a high-spin Fe^{IV}=O intermediate, pending further characterization. The ring expansion of the substrate is initiated by H-atom abstraction by the Fe^{IV}=O oxidant from one of the C2-methyl groups to form a carbon radical (Scheme 6). Sulfur migration to this carbon with concomitant homolytic cleavage of the C2–S bond results in ring expansion and shifts the radical site to the more stable tertiary C2 atom. Abstraction of an H-atom from C3–H generates a double bond between C2 and C3 (Scheme 6). When the C3–H is deuterated, the C2-hydroxylated product is formed in place of the desaturated product [69]. Crystal structures of DAOCS were obtained showing the binding of either substrate or α-KG in the same pocket [70], leading to the initial speculation of a ping-pong-type mechanism to accommodate the crystallographic results. However, more recent data provided evidence for the formation of a ternary DAOCS·α-KG·penicillin *N* complex, showing that DAOCS does follow the consensus mechanism for the action of α-KG-dependent oxygenases [68] (Scheme 3).

CAS is an α-KG-dependent enzyme representative of those that perform oxidative cyclization. It is actually quite an interesting enzyme in that it performs three different reactions in the biosynthesis of the β-lactamase inhibitor clavulanic acid—hydroxylation, heterocyclic ring formation, and finally desaturation (reaction b in Scheme 2), where the first reaction is separated from the latter two by a hydrolysis step that removes the guanyl group. Only the heterocyclic ring formation will be discussed here. Magnetic circular dichroism (MCD) studies on the CAS reaction sequence by Solomon and coworkers revealed that the 6-coordinate iron center in the resting enzyme becomes 5-coordinate upon binding α-KG as a bidentate ligand and the substrate [71]. This conclusion was corroborated by crystallographic data for binary CAS·α-KG and ternary CAS·α-KG·substrate complexes [72]. At this stage, the iron center would be poised to bind O_2 to generate the Fe^{IV}=O intermediate responsible for the three different oxidative transformations associated with this enzyme.

A crystal structure of the quaternary CAS·α-KG·substrate·NO complex (PDB ID: 1GVG) was reported 2 years later [73]. Because NO can be considered as an O_2 surrogate, this structure could provide insight into the step

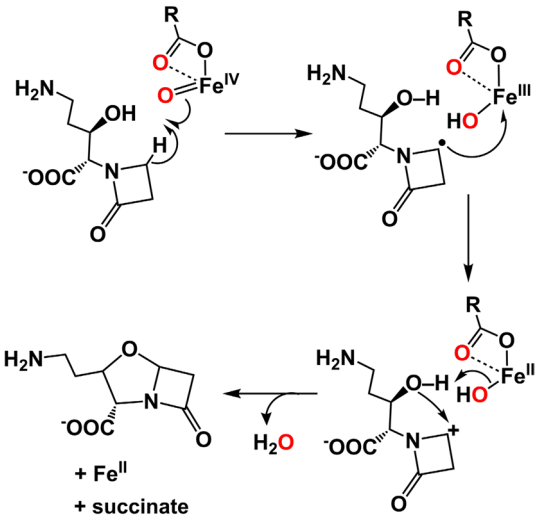

Scheme 7 Plausible pathway for the heterocyclic ring formation step of CAS

just prior to O_2 activation. Surprisingly, this structure shows a difference in the α-KG binding mode, where the carboxylate of α-KG switches from being *trans* to His144 in the ternary complex to being *trans* to His279 in the quaternary complex such that NO occupies the position *trans* to His144. This ligand rearrangement shows that there is some flexibility in the enzyme active site. However, an oxo *trans* to His144 would be improperly positioned to attack the target C–H bond on the substrate; based on these two structures of CAS complexes, an oxo *trans* to His279 would appear to be more effective for H-atom abstraction from the bound substrate. Thus, either the structure obtained for the quaternary CAS·α-KG·substrate·NO complex is mechanistically irrelevant or the oxo atom shifts to the position *trans* to His279 following O–O cleavage. A similar ferryl flip has been proposed for the halogenase WelO5 [74], which is discussed in "α-KG-dependent Halogenases" section.

Unlike the other α-KG-dependent enzymes discussed above, the Fe^{IV}=O oxidant for CAS has thus far not been trapped and characterized. All three transformations catalyzed by CAS likely share the same initial step of H-atom abstraction from the substrate C–H bond to be functionalized [75]. Then the nascent carbon radical for each of the three steps catalyzed by CAS goes down different paths: oxygen rebound for the first reaction, cyclization with the substrate hydroxyl group for the second reaction, and loss of the H-atom adjacent to the radical site to form the double bond in the third reaction (reaction b in Scheme 2). The mechanism to form the five-membered oxazolidine ring remains unclear. The mechanistically most straightforward hypothesis is shown in Scheme 7, in which the nascent substrate radical transfers an electron to the Fe^{III} center to generate a carbocation that is stabilized by the adjacent lactam N atom [75]. Subsequent nucleophilic attack of the hydroxyl group on the carbocation forms the heterocyclic five-membered ring. Other mechanistic options involving formation of a substrate alkoxyl radical have also been proposed [20, 76].

SnoK is another α-KG-dependent enzyme that catalyzes oxidative ring formation (Scheme 5, reaction a). Its crystal structure with a bound α-KG was recently reported [61]. When the substrate is modeled into its active site, the two carbons that form a bond, namely the C5″-atom of the amino sugar and the C2-atom of the anthracycline ring, are found to be closest to where the Fe^{IV}=O intermediate most likely forms. Hence it appears reasonable that a substrate radical would be generated at C5″ by the Fe^{IV}=O and the radical then forms a bond with the aromatic C2 to generate the ring and a radical site at C3; subsequent abstraction of the H-atom from C2 by the nascent Fe^{III}–OH moiety would then re-establish the aromaticity of the ring. This is a relatively new enzyme and further study is required to uncover its mechanism, which should be facilitated by the fact that SnoK only performs the ring formation reaction.

E. Epoxidation

Although epoxidation is a common reaction catalyzed by cytochromes P450, there are considerably fewer examples among nonheme iron enzymes. AsqJ, DdaC, and PenD are three α-KG-dependent oxygenases that perform C=C bond epoxidation on their respective native substrates [77–79]. Apart from these, thymine hydroxylase was shown to carry out epoxidation on a substrate analog with a vinyl group in place of the target methyl group [80]. In this section, we focus on AsqJ (reaction d2 in Scheme 2) [77]. AsqJ is a bifunctional enzyme that performs a desaturation reaction on the substrate followed by the epoxidation of the nascent double bond formed in the preceding step; both steps require α-KG and O_2 [77, 81]. The desaturation reaction to form the double bond is proposed to follow the mechanism presented in Section B where two consecutive H-atom abstractions are carried out by the initially formed Fe^{IV}=O unit and the resulting Fe^{III}–OH species.

Recent Mössbauer spectroscopic studies on AsqJ have provided evidence for the formation of an $S = 2$ Fe^{IV}=O intermediate with parameters similar to those of the other ferryl intermediates [39] (Table 1). Decay of the high-valent intermediate in the presence of the alkene substrate gave rise to an iron(II) center, consistent with the two-electron oxidation of the substrate C=C bond. Chemical quench experiments showed that the Fe^{IV}=O decay was connected to the formation of the epoxide product.

An intriguing observation was made when the reaction was carried out with $^{18}O_2$ using the native substrate or a substrate analog that was oxidized more slowly and

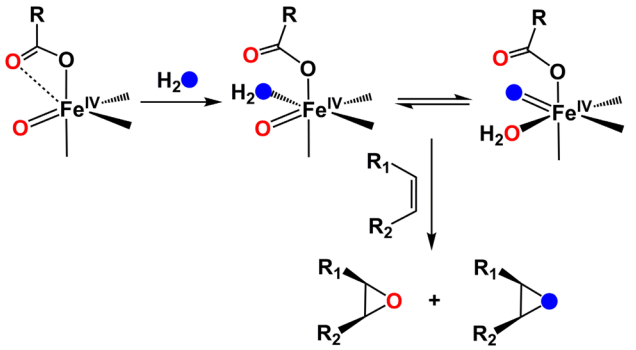

Scheme 8 Probable mechanism for O-isotope label exchange at the iron(IV) center of AsqJ via oxo-hydroxo tautomerism in the course of substrate epoxidation

resulted in a greater accumulation of the Fe^{IV}=O species. The slower the reaction or the larger the accumulation of the Fe^{IV}=O species, the less ^{18}O was incorporated into the product [39]. This result suggested the presence of a rapid oxo–hydroxo tautomerism of the Fe^{IV}=O species before substrate attack (Scheme 8), as previously proposed by Meunier for synthetic heme complexes [82]. Although it has not been observed before for other α-KG-dependent enzymes, solvent exchange into the Fe^{IV}=O unit has been demonstrated for nonheme model complexes [83, 84]. For the latter, it is proposed that water binds to the iron center in the Fe^{IV}=O state followed by proton transfer and deprotonation with assistance from surrounding H-bonding H_2O molecules [83]. A similar mechanism can be pictured for the enzyme. From the crystal structure of the nickel-substituted enzyme in complex with the desaturated substrate (PDB ID: 5DAV), the metal center is observed to be coordinated to the 2-His-1-carboxylate triad and a tridentate Tris buffer molecule that occupies the other three sites to form a six-coordinate metal center. Hence in the Fe^{IV} state, the Tris buffer molecule is presumably replaced by the oxo, the succinate (from the oxidative decarboxylation of α-KG) and a water molecule that can participate in the oxo–hydroxo tautomerism.

F. Endoperoxide formation

Fumitremorgin B endoperoxidase (FtmOx1) is a distinct member of the family of α-KG-dependent enzymes, as it catalyzes the unique reaction of forming an endoperoxide (reaction f in Scheme 2) [85, 86]. Crystallographic studies of FtmOx1 reveal a typical nonheme iron active site [87], as shown in Fig. 3, which displays a composite image based on the structures of the FtmOx1·α-KG and the FtmOx1·substrate complexes. More interestingly, Y224 is found to be positioned between the iron and the substrate and may thus play a role in the mechanism.

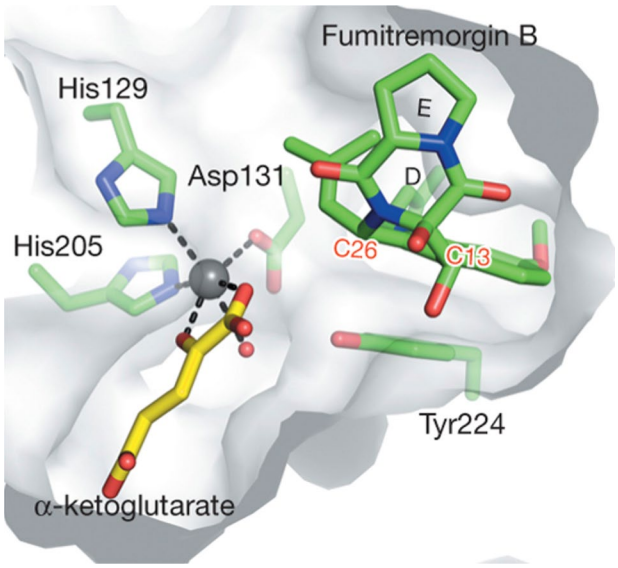

Fig. 3 Composite view of the FtmOx1·α-KG·substrate complex generated by superimposing structures of the E·S (PDB-4ZON) and E·α-KG (PDB-4Y5S) complexes. Atom *color code gray* = iron; *blue* = nitrogen; *red* = oxygen; *green* = enzyme residue and substrate carbon; *yellow* = α-KG carbon (reprinted with permission from Ref. [87]) (copyright from Nature Publishing Group)

RFQ-EPR experiments along with stopped-flow UV–visible spectroscopy and chemical quench experiments demonstrated the formation and decay of a tyrosyl radical within the same time frame as that of substrate consumption or product formation [87]. These results suggest formation of an Fe^{IV}=O species that oxidizes Y224 to its 1–e^--oxidized state concomitant with the appearance of a high-spin Fe^{III} EPR signal. The tyrosyl radical then abstracts the H-atom from the allylic C21–H bond of the substrate to generate a stabilized carbon radical that in turn reacts with O_2 to form the endoperoxide end product (Scheme 9). The native product of the enzyme has a secondary alcohol group (on the carbon marked with an asterisk in the structure of the product in Scheme 2f); under the reaction conditions used, the native product undergoes a further 2–e^- oxidation to afford a ketone as the major product rather than the alcohol. Most likely in the cell, there is a reductase or some other source of electrons to carry out this function. Y224 plays a key role in this reaction, as Y224A and Y224F variants deviate from the course of the native reaction and mainly carry out *N*-dealkylation of the indole nitrogen of the substrate. The Y224A variant can also effect hydroxylation of the isobutenyl side chain. Thus, in the absence of Y224, FtmOx1 performs transformations more commonly associated with α-KG-dependent enzymes.

The reactivities of the α-KG-dependent enzymes discussed above demonstrate their versatility and rich oxidation chemistry. The α-KG co-substrate undergoes

Scheme 9 Proposed mechanism for endoperoxide formation by FtmOx1

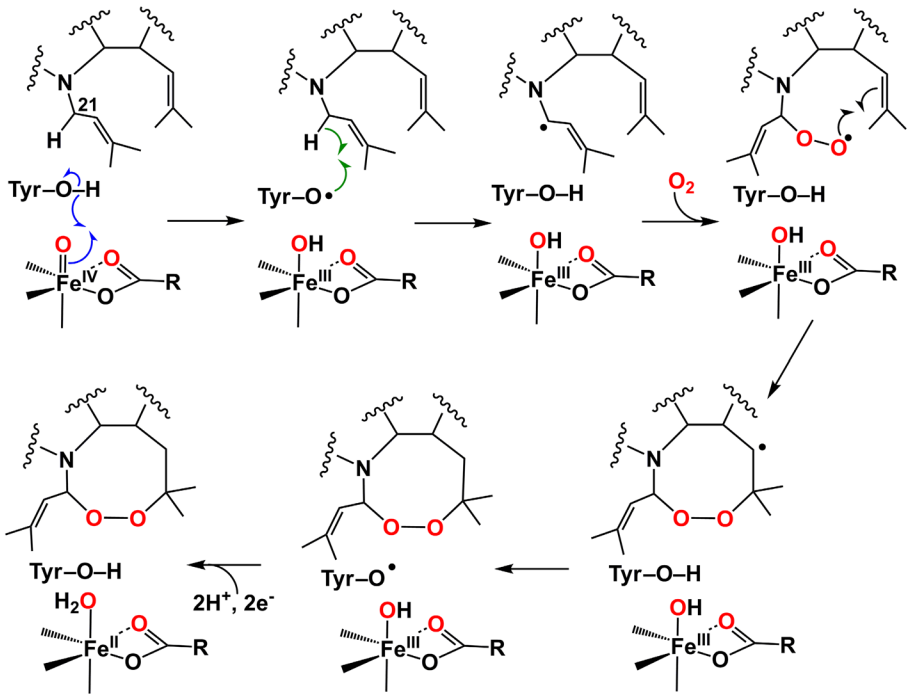

2–e⁻-oxidative decarboxylation to generate the Fe^{IV}=O oxidant that in turn oxidizes the substrate. In a few cases, such as 4-hydroxyphenylpyruvate dioxygenase (HPPD), 4-hydroxymandelate synthase (HMS), and CloR, the α-keto acid moiety is integrated into the substrate itself, such that an intramolecular version of the oxidative decarboxylation/substrate hydroxylation combination takes place upon exposure to O_2. These enzymes are discussed in the review by Peck and van der Donk in this special issue, which focuses on nonheme iron enzymes that carry out 4–e⁻-oxidations of substrates [88]. Yet another interesting group of enzymes are those that catalyze the halogenation of unactivated C–H bonds, which are discussed in the following section.

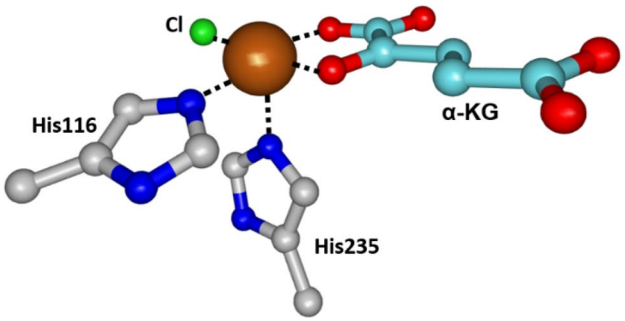

Fig. 4 Active site of SyrB2 complexed with α-KG and chloride ion (PDB ID: 2FCT). Atom *color code brown* = iron; *blue* = nitrogen; *red* = oxygen; *gray* = enzyme residue carbon; *light blue* = α-KG carbon; *green* = chloride

2. α-KG-dependent Halogenases

α-KG-dependent halogenases are nonheme iron enzymes that carry out the halogenation of relatively inert aliphatic C–H bonds in the biosynthesis of halogenated natural products [89]. They differ from the enzymes discussed in the previous section with respect to the iron active site. Instead of the 2-His-1-carboxylate triad commonly found among mononuclear nonheme iron enzymes, the iron centers in this subclass have a halide ligand that takes the place of the carboxylate ligand in the facial triad. This ligand substitution was first established in the crystal structure of the SyrB2-α-KG-Cl complex [90] (Fig. 4) and has been corroborated in the three halogenases subsequently crystallized, namely CytC3 [91], Cur Hal [92], and WelO5 [74].

The most extensively studied halogenase enzyme is SyrB2, which is involved in the biosynthesis of the natural product syringomycin E [43, 44, 90, 93, 94]. It chlorinates an L-threonine residue that is attached to the carrier protein SyrB1 via a thioester linkage, an essential transformation for the anti-fungal activity of syringomycin E. Comparison of the SyrB2 active site with those of other α-KG-dependent nonheme iron enzymes reveals that Ala118 has replaced the Asp or Glu residue of the 2-His-1-carboxylate motif [90], thereby providing enough space for a halide ion to bind the iron center. The lack of halogenation activity in A118E and A118D variants supports

the role A118 plays in allowing halide binding to the iron center.

Bollinger, Krebs, and co-workers have performed extensive studies to elucidate the mechanism of halogenases [42, 43]. Introduction of O_2 into an anaerobic solution containing SyrB2, Fe(II), α-KG, Cl^-, and the substrate L-Thr-SyrB1 elicited an increase in absorbance at around 318 nm, a feature typically observed for the Fe^{IV}=O intermediates observed for other α-KG-dependent enzymes [12]. Mössbauer spectroscopy confirmed this species to be a high-spin ($S = 2$) Fe^{IV} complex. EXAFS analysis of the same intermediate revealed an Fe–O distance of 1.66 Å and an Fe–Cl distance of 2.31 Å, identifying the intermediate to be a Cl–Fe^{IV}=O species [43]. For comparison, similar studies on the Br–Fe^{IV}=O intermediate of CytC3 showed an Fe–O distance of 1.62 Å and an Fe–Br distance of 2.43 Å [42]. Synchrotron-based nuclear resonance vibrational spectroscopic (NRVS) studies on the halo-ferryl intermediates of SyrB2 by Solomon and co-workers identified Fe-based vibrational modes that support a trigonal bipyramidal geometry for the high-valent iron center with an axial oxo atom and a halide ligand in the trigonal plane [44]. This description has been corroborated by subsequent MCD studies of the halo-ferryl intermediate of SyrB2-Br [95], which show spectral features that resemble for the most part those observed for a synthetic $S = 2$ Fe^{IV}=O complex that has been crystallographically characterized to be trigonal bipyramidal [96, 97]. This proposed structure of the iron(IV)-oxo intermediate is closely related to that favored by Sinnecker et al. for TauD-***J*** on the basis of DFT calculations where the monodentate halide is replaced by a bidentate Asp carboxylate [32].

Interestingly, unlike the ferryl intermediates of TauD and P4H, the Cl/Br–Fe^{IV}=O intermediates of CytC3 and SyrB2 exhibit two Mössbauer quadrupole doublets with isomer shifts of ~0.23 and ~0.30 mm s^{-1} (Table 1). The intensity ratios of these two doublets depend on the enzyme, the halide, the substrate-carrier protein, and the substrate: a ~ 1:1 ratio for CytC3-Cl/CytC2-L-Aba [41], a ~ 3:1 ratio for CytC3-Br/CytC2-L-Aba [42], and a ~ 1:4 ratio for SyrB2-Cl/SyrB1-L-Thr [43]. The nature of the two Fe^{IV} species for the halogenases and why the ratio varies have not been clarified. One computational study suggested that the two species may correspond to positional isomers of the Cl–Fe^{IV}=O unit where the oxo and chloride swap binding sites [98], while a more recent NRVS/DFT study by Solomon and coworkers proposed that the two forms arise from differences in H-bonding [44].

The reaction mechanism for the halogenases follows the paradigm associated with other α-KG-dependent enzymes in which the Fe^{IV}=O moiety of the halo-ferryl intermediate abstracts an H-atom from the carbon atom to be functionalized. A large ^{2}H-KIE of ~20 was observed for the decay of the Cl–Fe^{IV}=O intermediate of SyrB2 when the deuterated substrate d_5-L-Thr was used, suggesting that C–H bond cleavage is the rate determining step in a single turnover reaction [43]. After this step, the SyrB2 mechanism deviates from that of TauD with respect to the fate of the nascent substrate radical. For TauD, the radical presumably undergoes rebound with the Fe^{III}–OH moiety to form the hydroxylated product. However, in the case of the halogenases, a *–cis–*HO–Fe^{III}–Cl moiety is formed upon H-atom transfer, so the substrate radical is presented with a choice in the subsequent step—whether to form a C–O bond or a C–halide bond. Not surprisingly, this choice can be modulated by steric and electronic factors.

Matthews et al. have demonstrated that SyrB2 is an excellent system to explore such questions, as analogs of the threonine substrate are available [43, 94]. With L-norvaline (L-Nva) (which has one additional carbon compared to L-Thr but no hydroxyl group) bound to SyrB1 as substrate, the C5-hydroxylated product was obtained, but deuterating all the C5-H atoms afforded the C4-chlorinated substrate as the major product, so deuteration at C5 of Nva not only affects the regioselectivity but also switches the chemoselectivity from hydroxylation to halogenation. Furthermore, the rate of decay for the SyrB2 ferryl intermediate in the presence of the native L-Thr-SyrB1substrate was quite slow at 0.07 s^{-1} at 5 °C versus 9.5 s^{-1} for L-Nva-SyrB1 which is comparable to that for TauD-***J*** with taurine (13 s^{-1}) [35]. These observations suggest that the positioning of the target C–H bond on the substrate in the active site relative to the iron center may play a major role in determining the outcome of the reaction (Scheme 10). It should also be noted that the strength of the C5–H in L-Nva is greater than that of the corresponding C4–H bond, but this difference does not seem to affect the outcome of the reaction, again suggesting that it is the position of the substrate that matters the most. Therefore, it seems that the enzyme sacrifices its H-atom abstraction ability to gain selectivity for halogenation.

On the basis of NRVS results on the high-valent intermediates of SyrB2 and associated DFT calculations [44, 95], Solomon proposed that the difference in the C–H bond cleaving reactivity originates from the orientation of the target C–H bond relative to the Fe^{IV}=O moiety. For the native substrate L-Thr-SyrB1, it was suggested that the Fe^{IV}=O unit is perpendicular to the scissile C–H bond and follows a π-pathway to generate the substrate radical, which is in closer proximity to the chloride of the *cis*-HO–Fe^{III}–Cl moiety. On the other hand, the Fe^{IV}=O uses a σ-pathway to cleave a methyl C–H bond of the non-native substrate L-Nva-SyrB1 to form a substrate radical closer to the -OH group (Scheme 10). These ideas were supported by HYSCORE data on SyrB2·α-KG·NO·substrate complexes obtained by Silakov et al., which provided an estimate of the distances and angles between the substrate deuterium atoms of the bound Thr or Nva and the Fe–NO center [99].

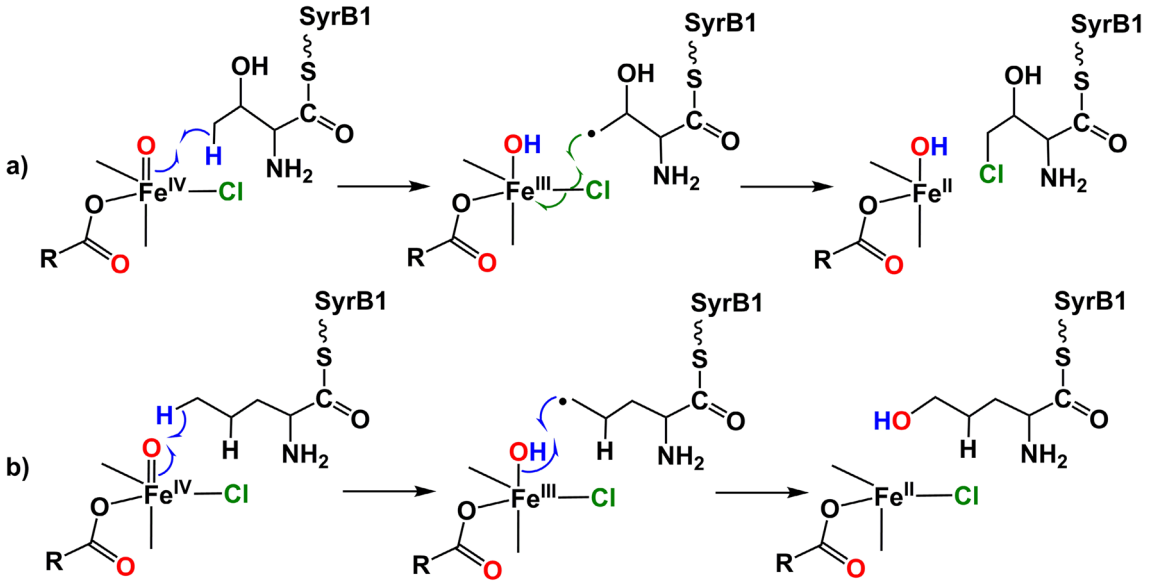

Scheme 10 Importance of substrate positioning of the scissile C–H bonds on SyrB2 substrates that lead to the distinct products, namely (**a**) halogenation for L-Thr-SyrB1 via a π-pathway and (**b**) hydroxylation for L-Nva-SyrB1 via a σ-pathway. For simplicity the histidine ligands on the Fe center are not shown

A very recent crystal structure of the halogenase WelO5 bound to α-KG and substrate sheds light on the effects of substrate orientation relative to the iron center [74]. This enzyme chlorinates the C13–H bond of 12-epifischerindole U and is the only halogenase characterized thus far with a substrate that is not required to be attached to a carrier protein. Its structure reveals that the target pro-*R* H-atom of C13 of the substrate points to the position of the presumed Fe^{IV}=O unit and away from the Fe–Cl bond (Fig. 5). This is further corroborated by the crystal structure of the quaternary enzyme·α-KG·substrate·NO complex (PDB ID: 5IQV) from which the oxo position can be predicted based on the location of NO. Assuming that this geometry is maintained at the Fe^{IV}=O stage, it would be difficult to justify the observed exclusive chlorination of the substrate. Indeed when G166 (located at the position of the carboxylate in corresponding α-KG-dependent oxygenases) is substituted with an aspartate, it occupies the Cl^- binding site, as shown by its crystal structure (PDB ID: 5IQU), and the G166D variant catalyzes substrate hydroxylation exclusively.

In order to rationalize the observed exclusive chlorination of the substrate by wild-type WelO5, it is proposed that a ligand rearrangement occurs such that the oxo ends up *trans* to His164 (instead of His259 as might be suggested by the crystal structure) (Fig. 5). The Fe^{IV}=O unit would thus be farther away from the substrate and hydroxylation would be disfavored. As mentioned earlier, a similar ligand rearrangement in the iron center to open a site for binding

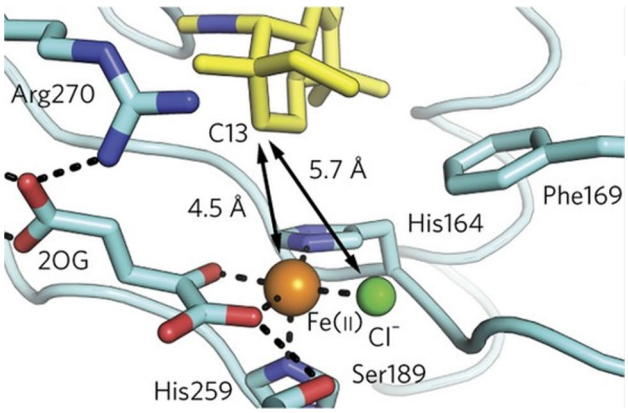

Fig. 5 Active site structure of WelO5 complexed with the substrate. (PDB ID: 5IQT). Atom *color code brown* = iron; *blue* = nitrogen; *red* = oxygen; *light blue* = enzyme residue and α-KG (or 2-OG) carbon; *yellow* = substrate carbon; *green* = chloride. Adapted from Ref. [74] with permission from Nature Publishing Group

NO was observed in CAS [73]. Additionally, Ser189 is found to be within H-bonding distance of the carboxylate of the α-KG; this residue may also H-bond to the putative Fe^{IV}=O *trans* to His164 to favor the rearrangement and regulate the selectivity. The importance of Ser189 is supported by the observation that the Ser189A variant affords a 1:1 ratio of R–OH and R–Cl products. Clearly more experiments are needed to shed light on these interesting mechanistic twists.

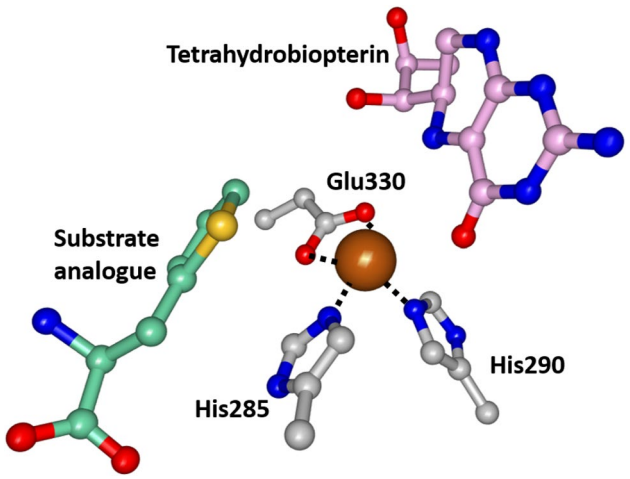

Fig. 6 Structure of PheH active site complexed with tetrahydrobiopterin and the substrate analog (3-(2-thienyl)-alanine) (THA) (PDB ID: 1MMK). Atom *color code brown* = iron; *red* = oxygen; *blue* = nitrogen; *gray* = carbon (enzyme residue); *light purple* = carbon (tetrahydrobiopterin); *light turquoise* = carbon (THA)

3. Pterin-dependent hydroxylases

Pterin-dependent hydroxylases are a small family of nonheme iron enzymes that perform hydroxylation of aromatic rings using O_2 and tetrahydrobiopterin (pterin or BH_4), which acts as a source for the two additional electrons required for completely reducing O_2. This family has three members—phenylalanine (PheH), tyrosine (TyrH), and tryptophan (TrpH) hydroxylase, all of which introduce a hydroxyl group at a specific position on the aromatic ring of the namesake amino acids. Each enzyme is involved in essential physiological functions. PheH is found mainly in liver and crucial for the metabolism of phenylalanine, converting it to tyrosine; TyrH converts L-tyrosine to L-DOPA and is vital for the biosynthesis of neurotransmitters like dopamine, norepinephrine, and epinephrine; and TrpH catalyzes the first step in the biosynthesis of another neurotransmitter, serotonin. Interestingly, these enzymes are able to hydroxylate native substrates of other family members albeit with different rates [100–102]. As many neurological and physiological diseases have been linked with irregular functioning of these enzymes, this family of enzymes has been reviewed extensively [14, 17–19, 102–104].

Crystal structures of all three enzymes confirm the presence of the 2-His-1-carboxylate motif that occupies three positions on the Fe^{II} center in the active site [105–107]. Additionally, the crystal structures of PheH with BH_4 and substrate analogs show that neither the substrate nor the cofactor BH_4 directly binds to the iron center [105, 108] (Fig. 6). However, substrate analog binding to the binary enzyme·BH_4 complex induces significant changes in the active site including (i) conversion of the iron center from 6-coordinate to 5-coordinate to open a site for binding O_2; (ii) moving the pterin cofactor closer to the Fe^{II} center, and (iii) changing the binding mode of the monodentate glutamate to bidentate. Spectroscopic studies on PheH complexes with native substrate and a cofactor analog further corroborate the structural changes in the active site mentioned above [109, 110]. Similar changes in the coordination geometry of the iron center in TyrH are observed in spectroscopic studies, suggesting a common O_2 activation pathway [111, 112]. These changes also affect the kinetics of the reaction with O_2, leading to the notion that multiple factors are working together to form the active oxidant in the correct sequence and orientation.

In 2007, Fitzpatrick, Bollinger, and Krebs trapped an Fe^{IV} intermediate in the catalytic cycle of TyrH. Its Mössbauer spectrum exhibited a doublet with an isomer shift (δ) of 0.25 mm s^{-1} and a quadrupole splitting ($|\Delta E_Q|$) of 1.27 mm s^{-1}, akin to those for other Fe^{IV}=O intermediates observed in other nonheme iron enzymes [46] (Table 1). The iron(IV) oxidation state was additionally confirmed by the formation of a high-spin Fe^{III} complex after cryoreduction of the Fe^{IV} intermediate as monitored by EPR. This Fe^{IV} intermediate reacted with L-tyrosine to form L-DOPA. In 2011, the corresponding PheH intermediate was found to have Mössbauer parameters similar to TyrH (δ = 0.28 mm s^{-1} and $|\Delta E_Q|$ = 1.26 mm s^{-1}), suggesting a common Fe^{IV}=O oxidant for this class of enzymes [45].

The first half of the proposed mechanism (Scheme 11) leading to formation of the ferryl intermediate remains unclear. While there is kinetic evidence for the formation of an intermediate preceding the formation of the Fe^{IV}=O species for PheH and TrpH, its nature has not been established [113, 114]. The proposed Fe^{II}–peroxy–BH_4 adduct is quite an attractive intermediate as it would avail of the electron donating properties of the tetrahydrobiopterin to bind O_2 by analogy to the reduced flavins [115] followed by or in concert with binding to the iron center in anticipation of the following O–O bond cleavage step to form the Fe^{IV}=O intermediate. It is also possible that O_2 first reacts with the Fe^{II} center to form an Fe^{III}-superoxo species that eventually reacts with BH_4 to form the Fe^{II}–peroxy–BH_4 complex. In addition, a peroxide shunt pathway where H_2O_2 is used in place of the BH_4 and O_2 to perform the hydroxylation of phenylalanine by all three enzymes has recently been demonstrated by Fitzpatrick and co-workers, reinforcing the notion that only the Fe^{IV}=O is involved in the hydroxylation part of the mechanism [116].

In the second half of the consensus mechanism (Scheme 11), an electrophilic attack on the aromatic ring by the Fe^{IV}=O intermediate is proposed. In support of this notion, the hydroxylation of site-specifically deuterated aromatic substrates by PheH and TrpH showed an inverse KIE and an NIH shift that suggest the formation of a

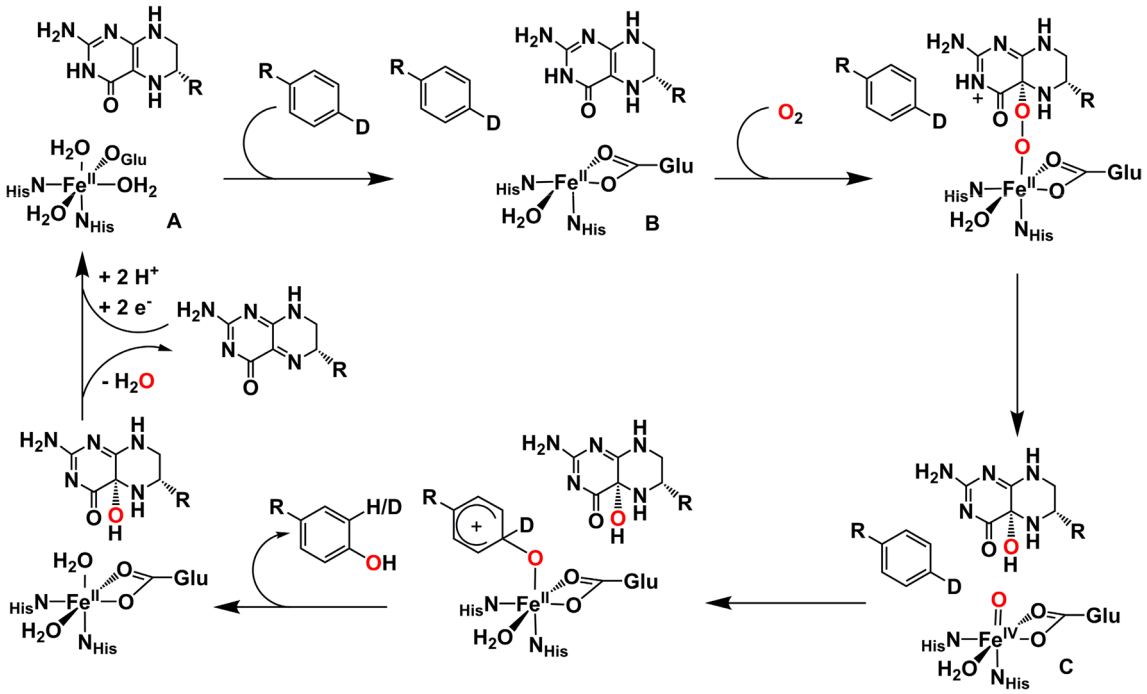

Scheme 11 Proposed mechanism for PheH, as representative of all pterin-dependent enzymes. Species A and B (with substrate analog) are crystallographically observed and species C was observed spectroscopically

cationic intermediate [100, 117] (Scheme 11). In addition, the reactions of TyrH with various *para*-substituted phenylalanines also exhibited a large negative value of ~ −4 for the Hammett parameter ρ, consistent with a highly electron-deficient transition state [101]. This family of enzymes can also perform hydroxylation of aliphatic C–H bonds on non-native substrates [118–120]. Nonclassical primary KIEs larger than 10 were found, implicating involvement of the Fe^{IV}=O intermediate in the H-atom abstraction, analogous to reactions catalyzed by α-KG-dependent iron enzymes discussed in an earlier section. The pterin-dependent hydroxylases represent another example of Nature's use of the same 2-His-1-carboxylate platform to generate similar active oxidants that perform different metabolically important transformations.

4. Rieske oxygenases

Rieske oxygenases are a class of nonheme iron enzymes that perform two-electron oxidations of substrates where a Rieske Fe_2S_2 cluster works in concert with the O_2-activating mononuclear nonheme iron center [7, 8, 14]. The two additional electrons required for complete O_2 reduction are supplied by NAD(P)H and delivered by a reductase to the iron center via a ferredoxin and the Rieske cluster. This is a versatile class of enzymes, and Scheme 12 provides a sampling of the variety of reactions they catalyze.

A unique transformation carried out by a large subset of enzymes in this class is the *cis*-dihydroxylation of aromatic C=C bonds (reaction a in Scheme 12), which is the first step in the biodegradation of aromatic molecules [7]. Both atoms of O_2 are incorporated into the products, so these enzymes are dioxygenases. To date, this is a reaction with only one synthetic precedent [121]. Other enzymes belonging to this class perform reactions that are more typical of monooxygenases such as *N*- and *O*-demethylation (reactions e and f in Scheme 12, respectively), *N*-oxidation (reaction b in Scheme 12), and hydroxylation of aromatic and aliphatic C–H bonds (reactions c and d in Scheme 12, respectively) [122–126]. Oxidative carbocyclization reactions have also been reported (reaction g in Scheme 12) [127].

Crystallographic data on several enzymes in this class reveal a mononuclear Fe^{II} center that is coordinated by the recurring 2-His-1-carboxylate facial triad motif [50, 122, 124, 128–132] (Fig. 7). This center is 44 Å away from the Rieske cluster found in the same subunit, but only 12 Å from the Rieske cluster of the adjacent subunit. Additionally, there is an aspartic or glutamic acid residue that has hydrogen bonding interactions with a His residue bound to the Rieske cluster and a His residue on the mononuclear iron center, providing a conduit for the two redox centers to communicate with each other. This notion was supported by an observed decrease in naphthalene dioxygenase (NDO) enzyme activity when Asp205, connecting the

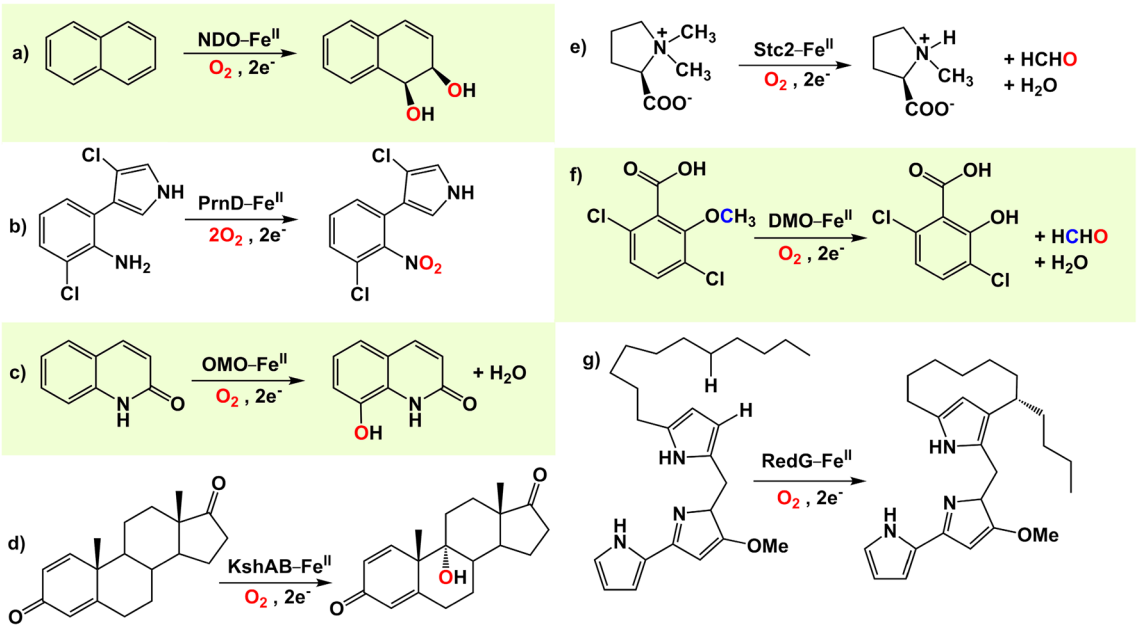

Scheme 12 Sampling of transformations catalyzed by Rieske oxygenases

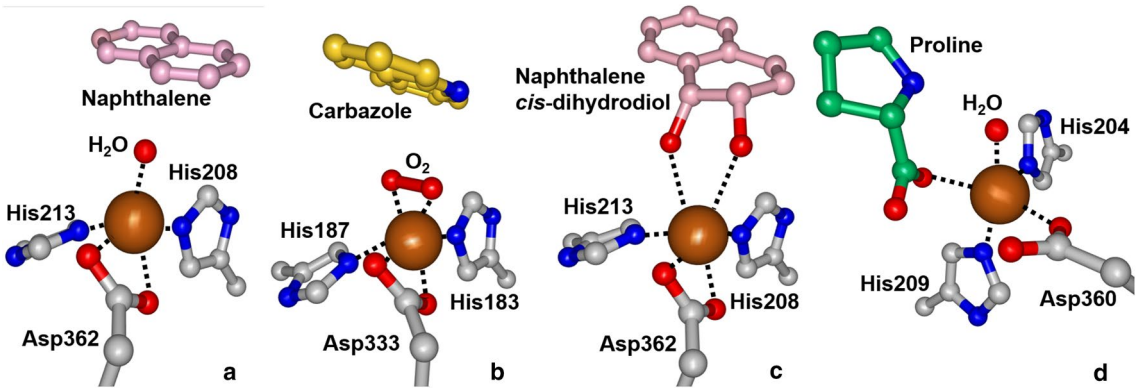

Fig. 7 Snapshots of the iron active site in Rieske oxygenases as it proceeds through the catalytic cycle. *Left to right* **a** NDO·substrate complex (PDB ID:1O7G); **b** CARDO E·S·O_2 complex (PDB ID:3VMI); **c** NDO·product complex (PDB ID:1O7P) and **d** Stc2·product complex (PDB ID:3VCP). Atom *color code brown* = iron; *blue* = nitrogen; *red* = oxygen; *gray* = enzyme carbon; *yellow* = carbazole carbon; *pink* = naphthalene carbon; *green* = proline carbon

Rieske cluster with the nonheme iron center, was replaced by other amino acids [133]. Furthermore, this substitution did not affect electron transfer from NADH to the Rieske cluster, so it must disrupt electron transfer between the Rieske cluster and the nonheme iron center. These results show that the nonheme iron center and the Rieske cluster of the adjacent subunit work together to form the functional unit that activates O_2.

Structural studies on NDO [50] and 2-oxoquinoline 8-monooxygenase (OMO) [124] show that their respective relatively hydrophobic substrates bind near, but not at, the nonheme iron center, which is five-coordinate and ligated to two His residues, a bidentate aspartate, and a solvent-derived ligand (Fig. 7a). A somewhat different picture is presented by stachydrine (*N,N*-dimethylproline) demethylase (Stc2) [122], as the substrate has a carboxylate functionality that can in principle bind to the iron center. Indeed the structure obtained for crystals of Stc2 incubated with substrate bears out this expectation but corresponds to that of a complex with the di-demethylated proline product (Fig. 7d). The proline carboxylate is in fact coordinated to the iron center as a monodentate ligand and trans

to a monodentate Asp360 (Fig. 7d). The observed proline binding mode places its N atom in close proximity to the adjacent water ligand, which is presumably displaced by O_2. The *N*-methyl groups of stachydrine would then be positioned well for attack by the bound O_2 or an oxidant derived therefrom in the subsequent *N*-demethylation step.

Crystal structures of E·S·O_2 adducts have been obtained for NDO and carbazole 1,9a-dioxygenase (CARDO) (Fig. 7b) and shed light on how O_2 can interact with the iron center [50, 51]. In both structures, O_2 binds in a side-on fashion at the position occupied by a water ligand in the enzyme-substrate complex. An O–O distance of 1.4–1.5 Å is found along with Fe–O distances in the range from 1.8 to 2.0 Å, values pointing to an iron(III)-peroxo species [52–54], which appears likely to be an intermediate in the catalytic cycle. Interestingly, a well-resolved water molecule is found within H-bonding distance to one of the atoms of the bound O_2 in the structure of the E·S·O_2 complex of CARDO [51], suggesting that this solvent molecule may serve as the source of the proton needed to facilitate cleavage of the O–O bond. Additionally for both enzymes, crystal structures of an enzyme·O_2 complex in the absence of substrate were obtained [50, 51], where O_2 binds in a side-on fashion in the case of NDO and in an end-on fashion in the case of CARDO. The mechanistic relevance of these species is not apparent at the present time. Last, Fig. 7c shows the structure of the NDO·product complex with the *cis*-dihydrodiol product bound in a bidentate fashion to the iron center, consistent with the transfer of dioxygen from substrate to product.

Mechanistically, the best understood of the Rieske enzymes are those that catalyze the *cis*-dihydroxylation of arenes, mainly stemming from the efforts of the Lipscomb laboratory. Kinetic studies show that O_2 activation occurs only when both the mononuclear iron center and the Rieske cluster are in their reduced states and in the presence of a bound substrate [134, 135], which should minimize unproductive use of reductant. The correct *cis*-diol products can also be generated in a single turnover from fully oxidized NDO and benzoate 1,2-dioxygenase (BZDO) by the addition of H_2O_2 instead of O_2 and two electrons, demonstrating the existence of an effective "peroxide shunt" pathway [49, 136]. Not surprisingly, the stoichiometric "peroxide shunt" reaction proceeds at a much slower rate than the catalytic O_2-dependent reaction. ^{18}O-labeling studies reveal that both O-atoms of H_2O_2 are incorporated into the NDO-derived diol product [136], raising the possibility of a common oxidant shared by the "peroxide shunt" pathway and the O_2 activation route of this dioxygenase.

Lipscomb and co-workers have trapped an intermediate in the "peroxide shunt" pathway for BZDO with Mössbauer features with $\delta = 0.50$ mm s^{-1} and $\Delta E_Q = 0.5$ mm s^{-1} and a negative zero field splitting [49]. The intermediate

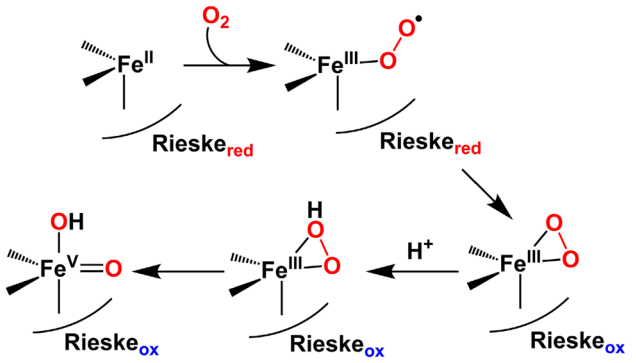

Scheme 13 Possible O_2-derived Fe-oxidants in Rieske oxygenases that can attack the substrate

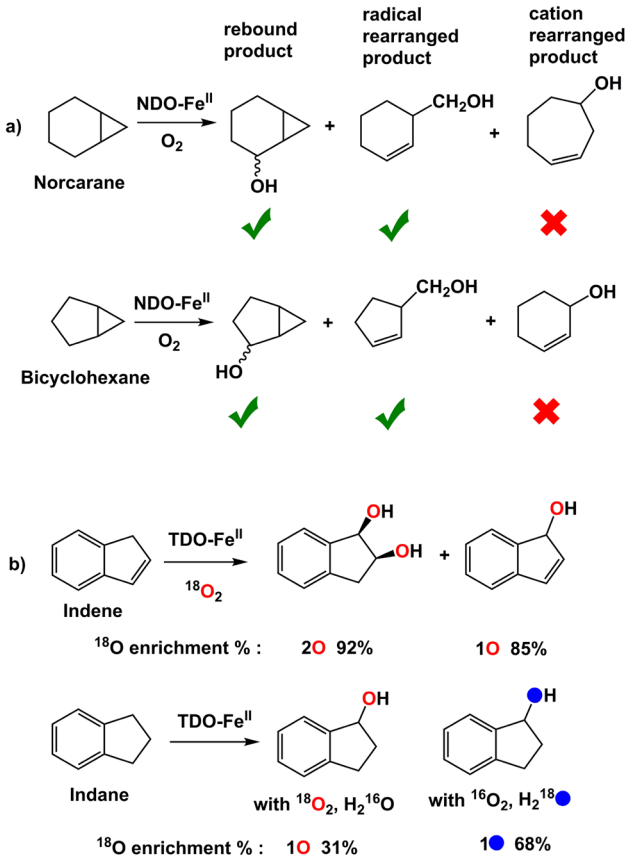

Scheme 14 **a** NDO-catalyzed oxidation of mechanistic probes norcarane and bicyclohexane showing which products are formed [137]; **b** ^{18}O-labeling results for TDO [138]

is proposed to be an $S = 5/2$ Fe^{III}–η^2-OOH species that likely corresponds to the crystallographically characterized E·S·O_2 adducts of NDO and CARDO [50, 51]. This side-on-bound Fe^{III}–OOH species may directly attack the substrate or undergo O–O bond cleavage to form an O=Fe^{V}–OH intermediate that then attacks the substrate (Scheme 13).

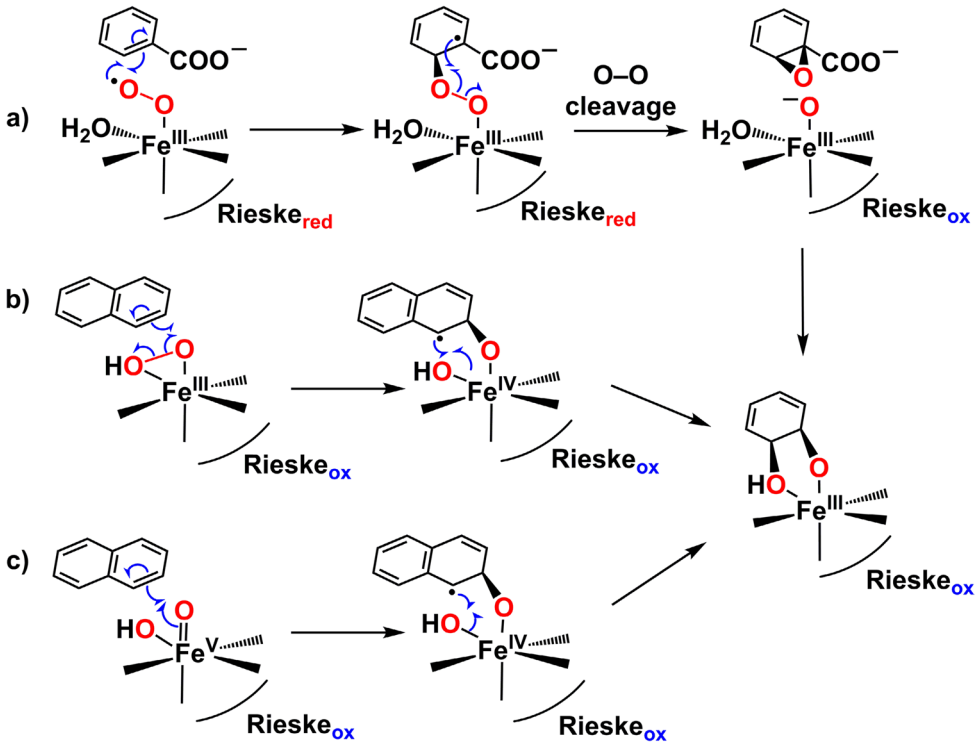

Scheme 15 Proposed mechanisms for *cis*-diol formation by Rieske oxygenases involving: **a** superoxoiron(III), **b** hydroperoxoiron(III) and **c** oxoiron(V) species as the active oxidant. For (**a**), the substrate is shown as benzoate, because evidence for an Fe^{III}–$O_2^{\cdot-}$ oxidant has been reported for BZDO. For (**b**) and (**c**), the substrate is naphthalene. For the product complex, only the *cis*-1,2-dihydrobenzene-1,2-diol structure common to both benzoate and naphthalene *cis*-dihydroxylation products is shown

Not much is known about what happens upon decay of the E·S·O_2 adduct, but some insight has been obtained from mechanistic studies of enzyme-catalyzed C–H bond oxidation. Besides naphthalene, NDO can oxidize norcarane and bicyclohexane, which are mechanistic probes for identifying radical versus cation intermediates (Scheme 14a). These substrates were found to afford rearranged hydroxylated products, consistent with the formation of a substrate radical intermediate [137]. ^{18}O-labeling studies on toluene dioxygenase (TDO) found that the substrate analog indene afforded 1-indenol and indan-1,2-diol products where ~90% of the O-atoms derive from $^{18}O_2$, but indane oxidation yielded 1-indanol with ~70% of the oxygen-atom deriving from water [138] (Scheme 14b). These experiments raise the possibility, at least for some substrates, that an intervening [Fe^{IV}(OH)···R·] species is involved during the reaction, which allows for the carbon radical rearrangement in the oxidation of radical clock substrates by NDO and isotope label incorporation from water in indane hydroxylation by TDO.

Recent studies on BZDO introduce an interesting twist to the evolving mechanism for the Rieske oxygenases. In single turnover kinetic studies of BZDO reacting with substituted benzoates and O_2, Lipscomb and co-workers found that the product formation rate correlated with the fastest phase of Rieske cluster oxidation and was sensitive to the electronic structure of the substrate [139]. These results lead to the postulation of a key role for the initial Fe-O_2 adduct in initiating substrate attack before electron transfer occurs from the reduced Rieske cluster to the mononuclear iron center (Scheme 13). In this drastically different scenario for *cis*-dihydroxylation, the initial Fe–O_2 adduct is formulated as an iron(III)-superoxo species that acts as an electrophilic oxidant, attacking the substrate to form an iron(III)-peroxy-substrate radical species. Electron transfer from the Rieske cluster leads to the cleavage of the O–O bond to form an arene oxide en route to the *cis*-diol product without involving any high-valent iron-oxo species (Scheme 15a). As proposed by Lipscomb [139], the *cis*-diol product would be formed in a stepwise process in which the epoxide ring is first opened up, perhaps by protonation, to generate a carbocation on the adjacent carbon atom that is then attacked by the Fe^{III}–O^- moiety from the same side as the initial superoxo attack, giving rise to the observed *cis*-diol product.

This new aromatic *cis*-dihydroxylation mechanism for Rieske dioxygenases clearly differs from earlier proposed mechanisms involving either an Fe^{III}–OO(H) (Scheme 15b) or an electrophilic HO–Fe^{V}=O oxidant (Scheme 15c) [14, 17]. Clearly, the superoxo-based mechanism cannot apply to the peroxide-shunt pathway, as the dioxygen moiety in the latter already contains one more electron equivalent than superoxide. It is also not clear whether the superoxo-based mechanism can be applied to reactions involving the cleavage of strong C–H bonds like those in Scheme 12, reactions d and g, as the C–H bond cleaving ability of an iron(III)-superoxo species has not been characterized in detail. However, C–H bond cleavage by such a species

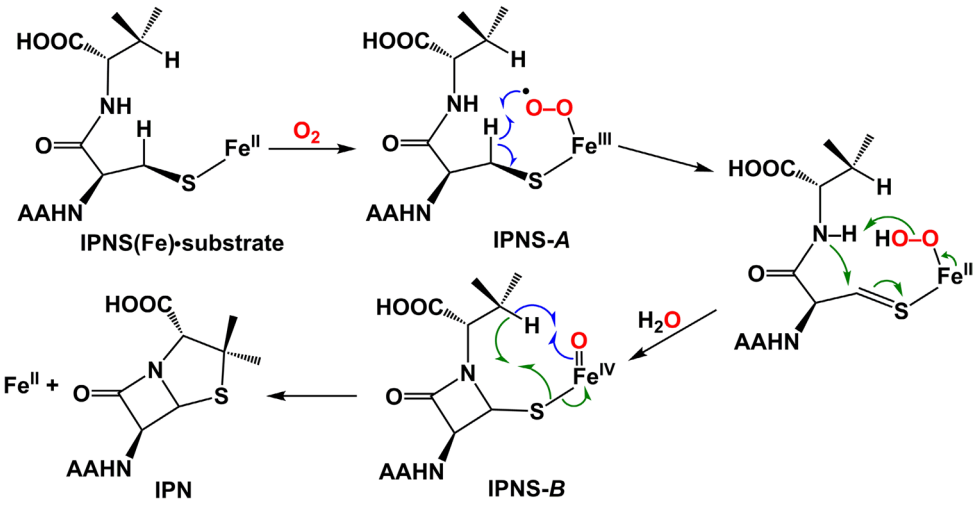

Scheme 16 Proposed mechanism for IPNS. For simplicity the ligands on the iron center are not shown. *Blue arrows* indicate the H-atom abstraction steps, while *green arrows* indicate ring formation steps. AA is the δ-(L-α-aminoadipoyl) moiety that is connected to the amino group of the cysteine of the substrate ACV

has been documented for IPNS, which is discussed in the next section. The possible involvement of an HO–Fe^{V}=O oxidant is supported by the existence of a few bona fide Fe^{V}=O complexes [140–143] and the mechanistic insights derived from studies on a number of bio-inspired nonheme iron catalysts [144–151].

5. Isopenicillin *N* synthase (IPNS)

Isopenicillin *N* synthase (IPNS) converts the tripeptide δ-(L-α-aminoadipoyl)-L-cysteinyl-D-valine (ACV) into the β-lactam antibiotic, isopenicillin *N* (IPN) [152] (Scheme 16). This reaction entails two consecutive oxidative cyclization steps to form the β-lactam and thiazolidine rings of the IPN product, each step being a 2–e^{-}-oxidative transformation. Thus only one O_2 is required to carry out this reaction.

The crystal structure of the IPNS·Fe(II)·ACV complex shows that IPNS belongs to the super-family of dioxygen activating mononuclear nonheme iron enzymes with a 2-His-1-carboxylate facial triad that binds the iron center (Fig. 8) [153]. The ACV substrate directly binds to the iron via the thiolate of the cysteine residue to generate a 5-coordinate iron center that is poised for O_2 binding (Scheme 16). Interestingly, this structure shows the open site for binding O_2 to be trans to the carboxylate of Asp216 of the 2-His-1-carboxylate facial triad, unlike most other nonheme iron enzymes in this family where O_2 binds trans to one of the two histidine residues of the facial triad motif [2]. This notion is corroborated by the crystal structure of the NO adduct of IPNS·Fe(II)·ACV. In addition, the NO oxygen atom is equidistant from both the valine nitrogen and the β-carbon of the cysteine, each of which loses an H-atom to form the β-lactam ring in the proposed mechanism (Fig. 8) [153].

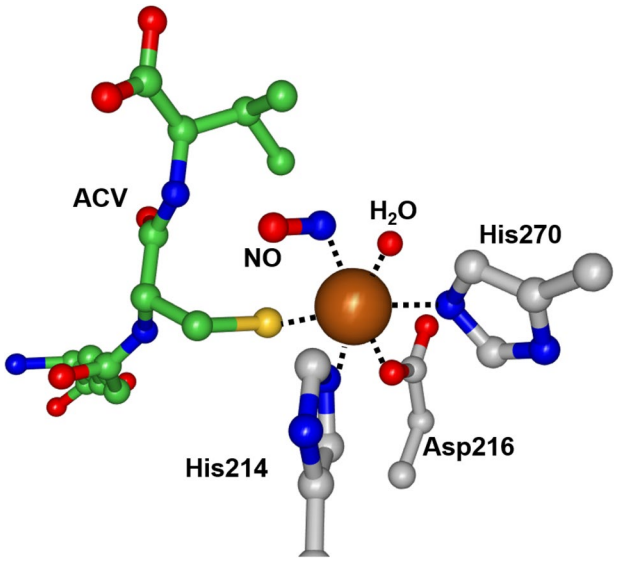

Fig. 8 Active site structure of IPNS complexed with substrate ACV and O_2 analog NO. (PDB ID:1BLZ) Atom *color code brown* = iron; *blue* = nitrogen; *red* = oxygen; *gray* = enzyme residue carbon; *yellow* = ACV sulfur; *green* = ACV carbon

Based on extensive mechanistic studies using substrate analogs [152, 154] and crystallographic studies of various enzyme complexes [153, 155] by Baldwin and co-workers, it has been established that the β-lactam ring is formed first followed by the thiazolidine ring, with the substrate anchored to the Fe center until the latter is formed. In the proposed mechanism, the initially formed O_2 adduct IPNS-***A*** abstracts a H-atom from the β-carbon atom of the cysteine of the ACV substrate to initiate the formation of the β-lactam ring and the Fe^{IV}=O species IPNS-***B*** that in turn cleaves the valine C_{β}–H bond leading to thiazolidine ring assembly (Scheme 16).

Scheme 17 Ethylene formation catalyzed by nonheme iron enzymes

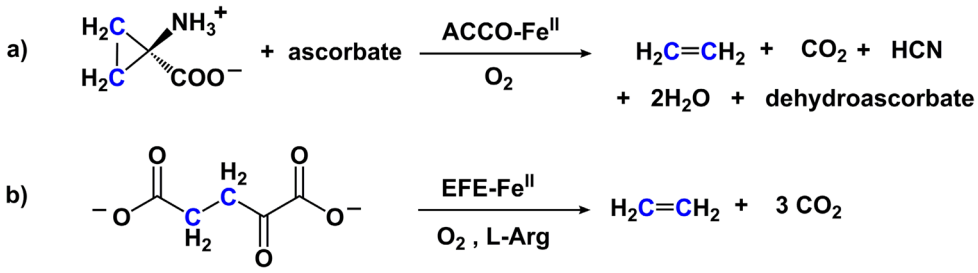

Recently, Bollinger, Krebs, and co-workers trapped these two intermediates by using selectively deuterated substrates to retard the respective C–H bond breaking steps and obtain their Mössbauer signatures [16]. Intermediate IPNS-***A***, obtained with the use of A[d_2-C]V (KIE ~ 17–33), is associated with a quadrupole doublet with $\delta = 0.53$ mm s^{-1} and $\Delta E_Q = 1.02$ mm s^{-1}. The observed isomer shift is typical of an $S = 5/2$ Fe^{III}(N/O) center, but the appearance of a quadrupole doublet indicates that this $S = 5/2$ center must be coupled to another paramagnetic moiety with half-integral spin, consistent with the assignment of IPNS-***A*** as an iron(III)-superoxo species. The broadening of the quadrupole doublet in weakly applied external magnetic fields suggests that the iron(III) center and the superoxo ligand are weakly coupled. These results show that the iron(III)-superoxo moiety of IPNS is capable of cleaving a C–H bond of moderate strength. Further support for the assignment of IPNS-*A* comes from its resemblance to the recently characterized first example of a synthetic iron(III)-superoxo complex, which exhibits a quadrupole doublet having $\delta = 0.58$ mm s^{-1} and $\Delta E_Q = 1.65$ mm s^{-1} [55]. Analysis of high-field Mössbauer spectra has established that the synthetic complex has an $S = 3$ ground spin state derived from weak ferromagnetic coupling of a high-spin ($S = 5/2$) iron(III) center with an $S = ½$ superoxide ligand [56]. This notion is additionally supported by the observation of a parallel mode EPR signal at $g = 8$ that is quite weak at 2 K but grows much more intense at 16 K, showing that it arises from the $M_S = \pm 2$ excited state of the $S = 3$ complex.

Intermediate IPNS-***B***, obtained with the use of AC[d_8-V] (KIE > 30), also exhibits a Mössbauer quadrupole doublet but with $\delta = 0.27$ mm s^{-1} and $\Delta E_Q = -0.44$ mm s^{-1}, parameters resembling those of $S = 2$ Fe^{IV}=O intermediates of other nonheme iron enzymes (Table 1) as well as those of a synthetic oxoiron(IV) complex with a thiolate ligand ($\delta = 0.19$ mm s^{-1} and $\Delta E_Q = 0.22$ mm s^{-1}) [156]. The mechanism for the formation of the C–S bond to make the thiazolidine ring is akin to that for the formation of the carbon-halogen bonds by halogenases; in both cases, the nascent carbon radical does not rebound to the resulting Fe^{III}–OH moiety, but rather forms a bond with the anionic ligand adjacent to the hydroxide on the iron center (Scheme 16). Computational studies agree with the conclusions from these experimental results [16, 157–159].

6. Enzymes that form ethylene

Ethylene is a hormone that plays an important role in the growth and development of plants [160, 161]. It is produced by nonheme iron enzymes such as 1-aminocyclopropane-1-carboxylate oxidases (ACCO) in plants and ethylene-forming enzymes (EFE) in plant-associated microbes [160, 162, 163] (Scheme 17). The latter has drawn recent interest as an alternative method for the production of ethylene from renewable sources [164–167].

ACCO is an enzyme typically found in plants that performs the oxidation of 1-aminocyclopropane-1-carboxylate (ACC) to ethylene, HCN, and CO_2 (Scheme 17a) [168]. The crystal structure of *Petunia hybrida* ACCO provides crystallographic proof that ACCO has an iron active site with a 2-His-1-carboxylate triad [169], as anticipated by observed sequence similarities to IPNS [4] and the family of α-KG-dependent enzymes [5]. The three residues occupy three of the six possible coordination sites of the iron(II) center. MCD studies of resting Fe^{II}-ACCO by Solomon and co-workers reveal that the iron(II) center is six-coordinate, suggesting that the three exogenous ligand sites are likely to be occupied by solvent water molecules [170]. Binding of ACC makes the iron(II) center five-coordinate, employing the same strategy as other nonheme iron enzymes in this super-family in making a coordination site available on the iron(II) center for binding O_2 after substrate binds [2, 21]. This five-coordinate configuration is observed when ACC is bound to the active site alone or in the presence of both ascorbate and HCO_3^-/CO_2, effector molecules needed for efficient catalytic production of ethylene [171–174].

EPR and ENDOR studies carried out by Hoffmann, Lipscomb, Que, and co-workers shed light on the binding of exogenous ligands such as substrate and O_2 [175, 176]. Following precedents established by Lipscomb in studies of other nonheme iron enzymes [177–181], NO has been employed as an O_2 surrogate that forms an adduct with the iron(II) center to generate an EPR-active $S = 3/2$

$\{Fe–NO\}^7$ unit. Indeed different $S = 3/2$ EPR signals are observed for the NO adducts of Fe^{II}-ACCO formed in the absence and in the presence of substrate, suggesting that both substrate and O_2 can bind simultaneously to the iron center, just like for many other nonheme iron enzymes. The same Fe^{II}-ACCO·substrate·NO adduct is formed either by addition of substrate to the pre-formed Fe^{II}-ACCO·NO complex or by reacting NO with Fe^{II}-ACCO in the presence of substrate. ENDOR studies with ^{17}O- and ^{15}N-labeled alanine (used as a substrate analog) provide persuasive evidence for bidentate binding of ACC to the iron center via the carboxylate and the amino group. On the other hand, formation of an Fe^{II}-ACCO·ascorbate·NO complex is not observed, suggesting that ascorbate does not bind to the iron center. More detailed ENDOR studies comparing the Fe^{II}-ACCO·NO and the Fe^{II}-ACCO·Ala·NO complexes based on ^{15}N-labeled ACCO and ^{17}O-labeled Ala samples have led to the proposal that NO likely binds trans to the Asp residue of the facial triad in the Fe^{II}-ACCO·NO complex but shifts to being trans to one of the His ligands upon binding of Ala. In the latter case, the alanine carboxylate binds trans to the Asp residue. The substrate and O_2 are thus bound cis to each other in the Fe^{II}-ACCO·ACC·O_2 complex, as demonstrated for other E·S·O_2 adducts in this super-family of enzymes where the substrate or co-substrate binds directly to the Fe^{II} center [14, 19–21, 182].

Ascorbate and HCO_3^-/CO_2 are small molecules that affect the chemistry of ACCO, but the above ENDOR results would appear to exclude them as ligands to the iron center. Efficient catalytic formation of ethylene requires the presence of both HCO_3^-/CO_2 and ascorbate [171–174, 183]. Under single turnover conditions, a sub-stoichiometric yield of ethylene can be generated without ascorbate but not without HCO_3^-/CO_2, so HCO_3^-/CO_2 must play an activator role [183]. Evidence favoring HCO_3^- (and not CO_2) as the form that likely interacts with ACCO derives from the observation that addition of anions such as nitrate and borate inhibits ethylene formation; indeed steady-state kinetic measurements have demonstrated borate to be a competitive inhibitor to HCO_3^-, with a binding affinity comparable to that of HCO_3^- [183]. It has been speculated that HCO_3^- may provide the proton that hydrogen bonds to the dioxygen moiety in the initial adduct to guide the reaction down its productive track [162, 183].

Ascorbate presumably plays the role of reductant in this reaction. Although it has been shown not to be absolutely required for ethylene formation under single turnover experiments, the iron center at the end of this reaction is in the +3 state [183], so the ascorbate is needed to regenerate the iron(II) center for the subsequent turnover. The ethylene formation rate in the single turnover experiments was found to be quite slow, but addition of ascorbate even at 10% of its K_M value significantly accelerated both iron oxidation and ethylene formation, suggesting that this reagent may also act as a high-affinity activator. In support of this idea, replacement of ascorbate by a redox-inactive structural analog of ascorbate, saccharic acid 1,4-lactone, resulted in a twofold acceleration of the ethylene formation rate but with no increase in ethylene yield [183]. Dilley and co-workers have also shown that the ascorbate analog 2,4-pteridinediol acts as a competitive activator of ACCO with respect to ascorbate, both exhibiting comparable binding affinities for ACCO [162]. Moreover, addition of 2,4-pteridinediol to ACCO in the absence of ascorbate produced some ethylene from ACC, so 2,4-pteridinediol can functionally replace ascorbate but is not as effective as ascorbate.

Kinetic isotope effect measurements by Klinman and co-workers have also shed light on the ACCO mechanism [184, 185]. Comparison of steady-state kinetic parameters of ACCO measured in H_2O and D_2O showed nearly identical solvent isotope effects (SIE) of ~2.3 for k_{cat}, k_{cat}/K_m(ACC), and k_{cat}/K_m(ascorbate), suggesting that hydrogen bonding interactions play an important role in the transition state. Moreover, an unusually large SIE of 5.0(9) was found for $k_{cat}/K_m(O_2)$, consistent with a rate determining hydrogen-atom transfer or proton-coupled electron transfer step in the activation of O_2. Most interestingly, a much larger $^{16}O_2/^{18}O_2$ kinetic isotope effect of 1.0215(5) was observed for $k_{cat}/K_m(O_2)$ of ACCO [185, 186], compared to values of 1.0054–1.0120 found for myoglobin, hemerythrin, TauD, and HppE. From this result, they have inferred a rate determining step for ACCO that entails a more significant change in the O–O bond order than for the others.

Possible mechanisms based on the above studies are collected in Scheme 18, wherein the oxidation of ACC to ACC$^\bullet$ is carried out by Fe^{III}–$O_2^\bullet$ (top), Fe^{III}– OOH (center), or Fe^{IV}=O (bottom) species. The notion of that an iron-bound superoxide can play an oxidant role in Scheme 18 (top) finds precedent in the work of Lipscomb and co-workers on the extradiol cleaving catechol dioxygenases [187, 188] and the Rieske dioxygenases [139] as well as in the recent work of Bollinger, Krebs, and co-workers on the first oxidation step of the IPNS reaction [16]. In the ACCO mechanism, this step entails H-atom transfer (HAT) from the NH_2 moiety of the substrate to the bound superoxide to generate Fe^{III}–OOH and ACC$^\bullet$. The function of ascorbate would then be to reduce H_2O_2 to water. In Scheme 18 (center), the initial Fe^{II}–O_2 adduct is reduced by ascorbate to generate Fe^{III}–OOH that abstracts an H-atom from the substrate amino group and undergoes O–O bond homolysis to generate an Fe^{IV}=O, which in turn gets reduced to Fe^{II}–OH_2. In Scheme 18 (bottom), O–O bond cleavage occurs first to generate the Fe^{IV}=O oxidant that abstracts an H-atom from ACC.

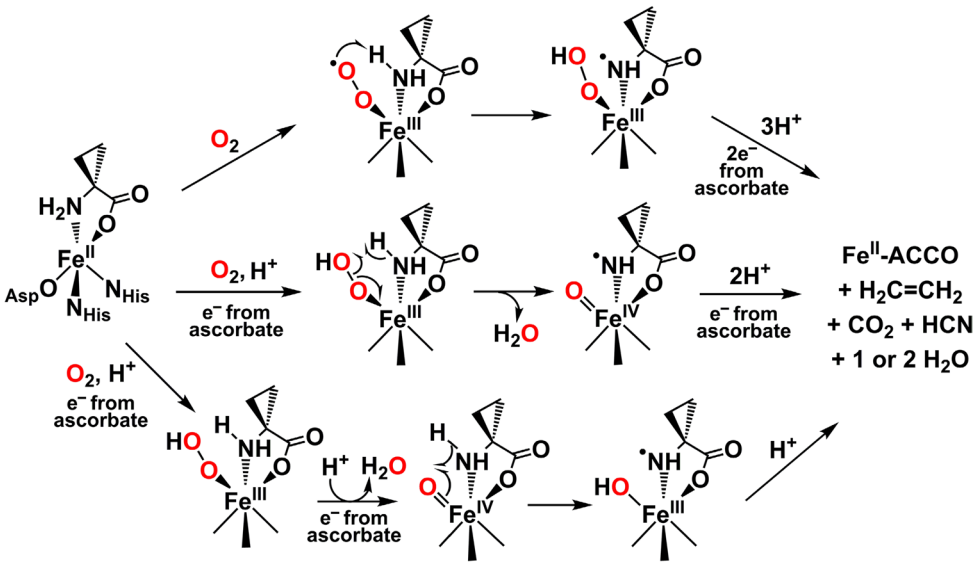

Scheme 18 Possible mechanisms for ACC oxidation by Fe^{II}-ACCO via putative Fe^{III}–$O_2^{\cdot}$ (*top*), Fe^{III}–OOH (*center*), or Fe^{IV}=O (*bottom*) oxidants

Dilley and co-workers have also presented evidence that the cyanide byproduct of the ACC oxidation reaction plays a role in modulating ACCO activity [162]. They found that the introduction of 0.1–1 mM cyanide increased ACCO activity, but addition of even higher concentrations of cyanide inhibited the enzyme. Additional experiments were performed with the ACC analog AIB (α-aminoisobutyric acid), which is oxidized by ACCO to form acetone, CO_2, and NH_3 but does not produce cyanide. Typically, ACCO oxidation of ACC decreased in rate during a 2-h incubation period due to enzyme inactivation; however, incubation of ACCO with AIB and cyanide prevented enzyme inactivation and its ACC oxidation activity was maintained/enhanced during the 2-h incubation period. Based on these observations, it was proposed that the cyanide byproduct remained bound to the iron(II) center at the O_2 binding site at the end of a reaction cycle and dissociated from the iron(II) center upon ascorbate binding near the active site, allowing O_2 to bind for the next turnover of the enzyme.

Less is known about the other example of an ethylene-forming enzyme, which is designated as EFE and found in plant-associated microbes such as *Pseudomonas syringae* pv. phaseolicola PK2 and *Penicillium digitatum*. Comparative sequence analysis and site-directed mutagenesis of EFE have led to the identification of H189, D191, and H268 as ligands that likely comprise the 2-His-1-carboxylate facial triad supporting the iron center [189]. The $HxDx_nH$ sequence pattern is similar to that found for the family of α-KG-dependent enzymes (see Table S1). In fact, α-KG is the actual substrate for this reaction and breaks down to form ethylene and three equivalents of CO_2 (Scheme 17b). It is proposed that these products are generated from the unobserved bicyclic alkylperoxoiron(IV) species in the generally accepted mechanism for the α-KG-dependent

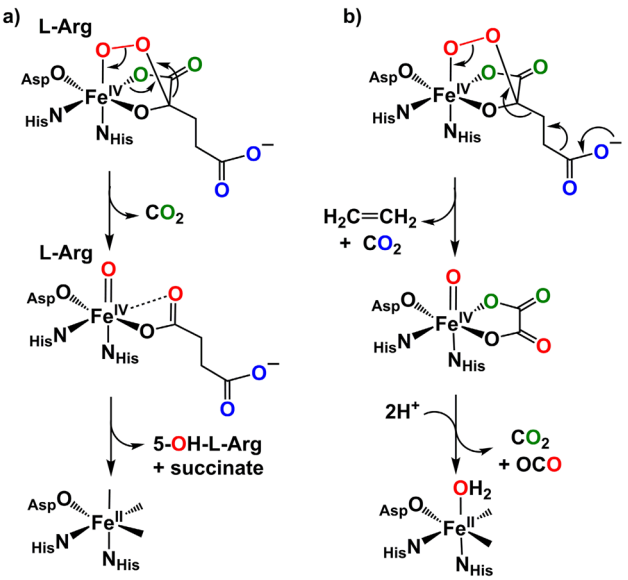

Scheme 19 Possible pathways for the decomposition of the bicyclic peroxoiron(IV) intermediate **a** to form succinate and the hydroxylated product and **b** to form ethylene and 3 CO_2. In (**b**) the conversion of the bound oxalate to 2 CO_2 is shown as a 2–e^- oxidation by the ferryl moiety. An alternative path involving oxo transfer from the ferryl moiety is also possible, but labeling experiments are needed to clarify this question

enzymes presented earlier in Scheme 3. However, instead of forming succinate and CO_2, this species breaks down via an alternative pathway that gives rise to the observed products (Scheme 19) [190].

Interestingly, ethylene formation by EFE requires the presence of L-Arg [163, 191, 192]. In fact, during the process, EFE also catalyzes the hydroxylation of L-arginine to 5-hydroxy-L-arginine, eventually forming

Scheme 20 Proposed mechanism for HppE

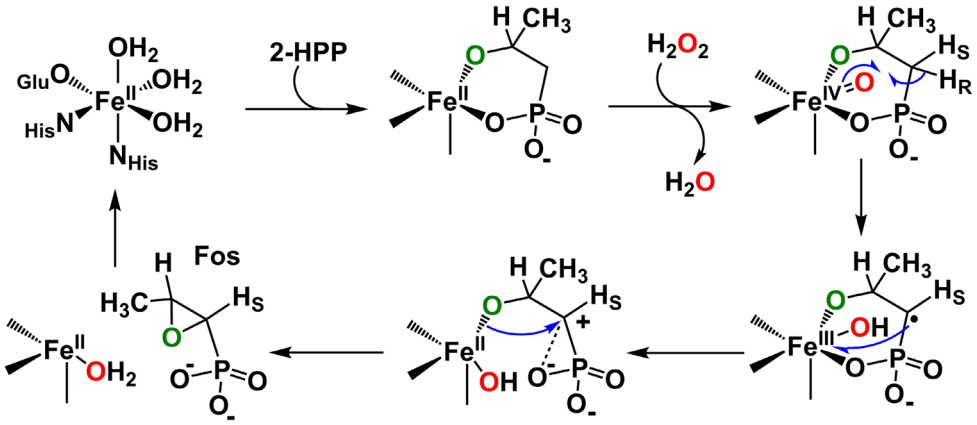

L-Δ^1-pyrroline-5-carboxylate (P5C) and guanidine in a subsequent non-enzymatic step [190]. At the same time, an equivalent amount of succinate is formed, suggesting that L-Arg hydroxylation follows the mechanism of a typical α-KG-dependent enzyme. Product analysis showed that ethylene formation was favored 2:1 over L-Arg hydroxylation.

Further studies by Hausinger and co-workers have lent support for the above mechanistic notions [190]. The use of L-Arg analogs led to ethylene formation without oxidation of the analogs themselves, while α-KG replacement by 2-oxoadipate resulted in the hydroxylation of L-Arg along with formation of glutarate, but with no generation of ethylene. It would thus appear that L-Arg binding is required to convert EFE into a form poised to bind O_2, as is typical for other α-KG-dependent enzymes (Schemes 3 and 19). L-Arg would be hydroxylated following the usual mechanism for such enzymes, but ethylene is formed by an alternative pathway in which the bicyclic peroxoiron(IV) intermediate decomposes to form ethylene, CO_2, and an oxalate bound to the oxoiron(IV) species (Scheme 19). In this case, the CO_2 formed derives from the terminal carboxylate of the α-KG, while the α-ketoacid unit is converted to oxalate, which is then oxidized by the Fe^{IV}=O moiety to generate two equivalents of CO_2 (Scheme 19). Further evidence will be required to support this novel mechanism. The most interesting question is how the alternative decay pathway for the bicyclic peroxoiron(IV) intermediate is facilitated by this particular active site.

7. (*S*)-2-Hydroxypropyl-1-phosphonate epoxidase (HppE)

(*S*)-2-hydroxypropyl-1-phosphonate epoxidase (HppE) catalyzes the last step in the biosynthetic pathway of the antibiotic fosfomycin, which involves an unusual 1,3-dehydrogenation of (*S*)-2-hydroxypropyl-1-phosphonate [(*S*)-2-HPP] to form an epoxide, namely fosfomycin [*1R,2S*-epoxypropylphosphonate] [193]. Unlike most of the products of enzyme reactions discussed in this review, the epoxide O-atom of fosfomycin does not derive from O_2, but originates from the secondary alcohol group of the substrate [194–196] (Scheme 20). Crystallographic studies show that HppE belongs to the family of nonheme iron enzymes with a 2-His-1-carboxylate facial triad and that the substrate binds to the iron center as a bidentate ligand via the C2-hydroxyl oxygen and a phosphonate oxygen [9]. The iron coordination environment of the E·S complex of HppE thus resembles that of the binary E·α-KG adduct formed in the first step in the mechanism for α-KG-dependent enzymes.

Despite the similarity, HppE differs mechanistically from its α-KG-dependent cousins such as AsqJ, DdaC, and PenD. Although initially thought to be a O_2-dependent enzyme, HppE has been demonstrated by Bollinger, Krebs, and Liu to be a peroxidase exhibiting a 1:1 H_2O_2:fosfomycin stoichiometry [197]. It is proposed that H_2O_2 reacts with the iron(II) center to form an Fe^{IV}=O oxidant that cleaves the target C–H bond to form a substrate radical. This radical, however, does not undergo rebound with the incipient Fe^{III}–OH unit but instead forms a C–O bond with the iron-ligated substrate alkoxide to afford the epoxide product (Scheme 20). This pathway may be favored by electron transfer from the substrate radical to the incipient Fe^{III}–OH center to generate a carbocation that is readily attacked by the nucleophilic alkoxide. Recent studies by Liu and co-workers using 1-hydroxypropylphosphonic acid ((R)-1-HPP) and its derivatives demonstrated a biologically unprecedented 1,2-phosphono migration, which is best rationalized by carbocation formation at C1 following H-atom abstraction by the proposed Fe^{IV}=O [198, 199]. Although this proposed mechanism is quite plausible based on precedents established by other nonheme iron enzymes, the proposed oxoiron(IV) intermediate has not yet been characterized to substantiate the mechanism. In addition, the C–O bond forming step in HppE may share common

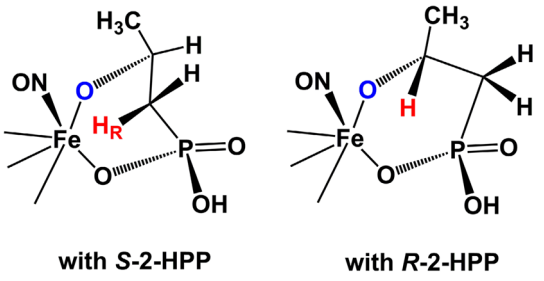

Fig. 9 Conformations of *S*-2-HPP and *R*-2-HPP when bound to the iron center of HppE resulting in the cleavage of different C–H bonds by the incipient Fe^{IV}=O (based on crystal structures and modeling studies of E·S·NO complexes with *S*-2-HPP and *R*-2-HPP. (PDB ID: 3SCF and 3SCG) [200]

mechanistic features with corresponding C-halide bond forming steps in the halogenases and the C–S bond forming step in IPNS in the assembly of the thiazolidine ring.

The reaction specificity of HppE is quite interesting. The natural substrate *S*-2-HPP gives rise to an epoxide product, but its enantiomer *R*-2-HPP is oxidized to a distinct ketone product. Comparison of the structures of Fe^{II}-HppE·NO complexes with bound *R*- or *S*-2-HPP shows that both substrates bind to the iron center in a bidentate fashion via the C2-hydroxyl and the phosphonate oxygen atom [200], but in different conformations such that distinct C–H bonds are oriented towards the putative Fe^{IV}=O oxidant (Fig. 9). So, for *S*-2-HPP the pro-*R* C1–H bond is cleaved to form the epoxide product, while for *R*-2-HPP a C2–H bond is broken to afford the ketone product.

8. Perspective

In this review, we provide a 20-year perspective of developments in the bioinorganic chemistry of dioxygen activating mononuclear nonheme iron enzymes that employ a common 2-His-1-carboxylate facial triad to bind the iron center. Members of this super-family have increased in number during this period, ballooning to over a hundred and catalyzing many different reactions. We have focused only on those enzymes that have been shown to form or likely to generate a high-valent iron-oxo oxidant, as other articles in this special issue cover related topics, such as the ring-cleaving dioxygenases by Wang et al. [201] and enzymes that carry out 4–e^--oxidations of substrates such as HPPD, HMS, and HEPD by Peck and van der Donk [88]. These 20 years have also seen great strides in our mechanistic understanding of these enzymes, including the trapping of reactive intermediates *in crystallo* or from solution with the use of rapid-freeze-quench techniques, including iron(III)-superoxo, iron(III)-peroxo, and iron(IV)-oxo species, compositely chronicling the step-by-step progress of the bound O_2 from initial adduct to high-valent oxidant. It is truly amazing that an active site motif as simple as the 2-His-1-carboxylate facial triad can serve as such a versatile platform on which to catalyze a diverse array of oxidative transformations. These enzymes further confirm Nature's ingenuity for inventing reactions as the need arises.

Acknowledgements We thank the U. S. National Science Foundation for funding (CHE-1361773 to L.Q.) and are grateful to Dr. Caleb Allpress and Dr. Johannes E. M. N. Klein for valuable input and discussions.

References

1. Hegg EL, Que L (1997) Eur J Biochem 250:625–629
2. Koehntop KD, Emerson JP, Que L (2005) J Biol Inorg Chem 10:87–93
3. Samson SM, Belagaje R, Blankenship DT, Chapman JL, Perry D, Skatrud PL, VanFrank RM, Abraham EP, Baldwin JE, Queener SW, Ingolia TD (1985) Nature 318:191–194
4. Roach PL, Clifton IJ, Fülöp V, Harlos K, Barton G, Hajdu J, Andersson I, Schofield CJ, Baldwin JE (1995) Nature 375:700–704
5. Prescott AG (1993) J Exp Bot 44:849–861
6. Aik WS, Chowdhury R, Clifton IJ, Hopkinson RJ, Leissing T, McDonough MA, Nowak R, Schofield CJ, Walport LJ (2015) In: Schofield CJ, Hausinger RP (eds) 2-Oxoglutarate-dependent Oxygenases. The Royal Society of Chemistry, Cambridge, pp 59–94
7. Ferraro DJ, Gakhar L, Ramaswamy S (2005) Biochem Biophys Res Commun 338:175–190
8. Barry SM, Challis GL (2013) ACS Catal 3:2362–2370
9. Higgins LJ, Yan F, Liu P, Liu H, Drennan CL (2005) Nature 437:838–844
10. Cicchillo RM, Zhang H, Blodgett JAV, Whitteck JT, Li G, Nair SK, Van Der Donk WA, Metcalf WW (2009) Nature 459:871–874
11. Smith JL, Khare D (2015) In: Schofield CJ, Hausinger RP (eds) 2-Oxoglutarate-dependent Oxygenases. The Royal Society of Chemistry, Cambridge, pp 401–413
12. Krebs C, Fujimori DG, Walsh CT, Bollinger JM (2007) Acc Chem Res 40:484–492
13. Bollinger JM, Chang W, Matthews ML, Martinie RJ, Boal AK, Krebs C (2015) In: Schofield CJ, Hausinger RP (eds) 2-Oxoglutarate-dependent Oxygenases. The Royal Society of Chemistry, Cambridge, pp 95–122
14. Kovaleva EG, Lipscomb JD (2008) Nat Chem Biol 4:186–193
15. van der Donk WA, Krebs C, Bollinger JM (2010) Curr Opin Struct Biol 20:673–683
16. Tamanaha E, Zhang B, Guo Y, Chang W, Barr EW, Xing G, St. Clair J, Ye S, Neese F, Bollinger JM, Krebs C (2016) J Am Chem Soc 138:8862–8874
17. Costas M, Mehn MP, Jensen MP, Que L (2004) Chem Rev 104:939–986
18. Abu-Omar MM, Loaiza A, Hontzeas N (2005) Chem Rev 105:2227–2252
19. Bruijnincx PCA, van Koten G, Klein Gebbink RJM (2008) Chem Soc Rev 37:2716–2744
20. Martinez S, Hausinger RP (2015) J Biol Chem 290:20702–20711
21. Solomon EI, Goudarzi S, Sutherlin KD (2016) Biochemistry 55:6363–6374

22. White MD, Flashman E (2016) Curr Opin Chem Biol 31:126–135
23. Schofield CJ, Hausinger RP (eds) (2015) 2-Oxoglutarate-dependent oxygenases. The Royal Society of Chemistry, Cambridge
24. Taabazuing CY, Hangasky JA, Knapp MJ (2014) J Inorg Biochem 133:63–72
25. Shen L, Song C-X, He C, Zhang Y (2014) Annu Rev Biochem 83:585–614
26. Mosammaparast N, Shi Y (2010) Annu Rev Biochem 79:155–179
27. Gorres KL, Raines RT (2010) Crit Rev Biochem Mol Biol 45:106–124
28. Hausinger RP (2004) Crit Rev Biochem Mol Biol 39:21–68
29. Hamed RB, Gomez-Castellanos JR, Henry L, Ducho C, McDonough MA, Schofield CJ (2013) Nat Prod Rep 30:21–107
30. Hanauske-Abel HM, Günzler V (1982) J Theor Biol 94:421–455
31. Price JC, Barr EW, Tirupati B, Bollinger JM, Krebs C (2003) Biochemistry 42:7497–7508
32. Sinnecker S, Svensen N, Barr EW, Ye S, Bollinger JM, Neese F, Krebs C (2007) J Am Chem Soc 129:6168–6179
33. Proshlyakov DA, Henshaw TF, Monterosso GR, Ryle MJ, Hausinger RP (2004) J Am Chem Soc 126:1022–1023
34. Riggs-Gelasco PJ, Price JC, Guyer RB, Brehm JH, Barr EW, Bollinger JM, Krebs C (2004) J Am Chem Soc 126:8108–8109
35. Price JC, Barr EW, Glass TE, Krebs C, Bollinger JM (2003) J Am Chem Soc 125:13008–13009
36. Proshlyakov DA, McCracken J, Hausinger RP (2017) J Biol Inorg Chem. doi:10.1007/s00775-016-1406-3
37. Hoffart LM, Barr EW, Guyer RB, Bollinger JM, Krebs C (2006) Proc Natl Acad Sci 103:14738–14743
38. Chang C-Y, Lyu S-Y, Liu Y-C, Hsu N-S, Wu C-C, Tang C-F, Lin K-H, Ho J-Y, Wu C-J, Tsai M-D, Li T-L (2014) Angew Chem Int Ed 53:1943–1948
39. Chang W, Li J, Lee JL, Cronican AA, Guo Y (2016) J Am Chem Soc 138:10390–10393
40. Chang W, Guo Y, Wang C, Butch SE, Rosenzweig AC, Boal AK, Krebs C, Bollinger JM (2014) Science 343:1140–1144
41. Galonić DP, Barr EW, Walsh CT, Bollinger JM, Krebs C (2007) Nat Chem Biol 3:113–116
42. Fujimori DG, Barr EW, Matthews ML, Koch GM, Yonce JR, Walsh CT, Bollinger JM, Krebs C, Riggs-Gelasco PJ (2007) J Am Chem Soc 129:13408–13409
43. Matthews ML, Krest CM, Barr EW, Vaillancourt FH, Walsh CT, Green MT, Krebs C, Bollinger JM (2009) Biochemistry 48:4331–4343
44. Wong SD, Srnec M, Matthews ML, Liu LV, Kwak Y, Park K, Bell CB, Alp EE, Zhao J, Yoda Y, Kitao S, Seto M, Krebs C, Bollinger J, Solomon EI (2013) Nature 499:320–323
45. Panay AJ, Lee M, Krebs C, Bollinger JM, Fitzpatrick PF (2011) Biochemistry 50:1928–1933
46. Eser BE, Barr EW, Frantom PA, Saleh L, Bollinger JM, Krebs C, Fitzpatrick PF (2007) J Am Chem Soc 129:11334–11335
47. Biswas AN, Puri M, Meier KK, Oloo WN, Rohde GT, Bominaar EL, Münck E, Que L (2015) J Am Chem Soc 137:2428–2431
48. Puri M, Biswas AN, Fan R, Guo Y, Que L (2016) J Am Chem Soc 138:2484–2487
49. Neibergall MB, Stubna A, Mekmouche Y, Münck E, Lipscomb JD (2007) Biochemistry 46:8004–8016
50. Karlsson A, Parales JV, Parales RE, Gibson DT, Eklund H, Ramaswamy S (2003) Science 299:1039–1042
51. Ashikawa Y, Fujimoto Z, Usami Y, Inoue K, Noguchi H, Yamane H, Nojiri H (2012) BMC Struct Biol 12:15
52. Li F, Meier KK, Cranswick MA, Chakrabarti M, Van Heuvelen KM, Münck E, Que L (2011) J Am Chem Soc 133:7256–7259
53. Cho J, Jeon S, Wilson SA, Liu LV, Kang EA, Braymer JJ, Lim MH, Hedman B, Hodgson KO, Valentine JS, Solomon EI, Nam W (2011) Nature 478:502–505
54. Roelfes G, Vrajmasu V, Chen K, Ho RYN, Rohde JU, Zondervan C, La Crois RM, Schudde EP, Lutz M, Spek AL, Hage R, Feringa BL, Münck E, Que L (2003) Inorg Chem 42:2639–2653
55. Chiang C-W, Kleespies ST, Stout HD, Meier KK, Li P-Y, Bominaar EL, Que L, Münck E, Lee W-Z (2014) J Am Chem Soc 136:10846–10849
56. Stout HD, Kleespies ST, Chiang CW, Lee WZ, Que L, Münck E, Bominaar EL (2016) Inorg Chem 55:5215–5226
57. Klein JEMN, Que L (2016) Encycl Inorg Bioinorg Chem. doi:10.1002/9781119951438.eibc2344
58. McDonald AR, Que L (2013) Coord Chem Rev 257:414–428
59. Neidig ML, Solomon EI (2005) Chem Commun 5843–5863
60. Usharani D, Janardanan D, Shaik S (2011) J Am Chem Soc 133:176–179
61. Siitonen V, Selvaraj B, Niiranen L, Lindqvist Y, Schneider G, Metsä-Ketelä M (2016) Proc Natl Acad Sci 113:5251–5256
62. Stapon A, Li R, Townsend CA (2003) J Am Chem Soc 125:15746–15747
63. Clifton IJ, Doan LX, Sleeman MC, Topf M, Suzuki H, Wilmouth RC, Schofield CJ (2003) J Biol Chem 278:20843–20850
64. Topf M, Sandala GM, Smith DM, Schofield CJ, Easton CJ, Radom L (2004) J Am Chem Soc 126:9932–9933
65. Borowski T, Broclawik E, Schofield CJ, Siegbahn PEM (2006) J Comput Chem 27:740–748
66. Phelan RM, Townsend CA (2013) J Am Chem Soc 135:7496–7502
67. Lloyd MD, Lee H-J, Harlos K, Zhang Z-H, Baldwin JE, Schofield CJ, Charnock JM, Garner CD, Hara T, Terwisscha van Scheltinga AC, Valegård K, Viklund JAC, Hajdu J, Andersson I, Danielsson Å, Bhikhabhai R. (1999) J Mol Biol 287:943–960
68. Tarhonskaya H, Szöllössi A, Leung IKH, Bush JT, Henry L, Chowdhury R, Iqbal A, Claridge TDW, Schofield CJ, Flashman E (2014) Biochemistry 53:2483–2493
69. Baldwin JE, Adlington RM, Crouch NP, Schofield CJ, Turner NJ, Aplin RT (1991) Tetrahedron 47:9881–9900
70. Valegård K, Terwisscha van Scheltinga AC, Dubus A, Ranghino G, Oster LM, Hajdu J, Andersson I (2004) Nat Struct Mol Biol 11:95–101
71. Zhou J, Kelly WL, Bachmann BO, Gunsior M, Townsend CA, Solomon EI (2001) J Am Chem Soc 123:7388–7398
72. Zhang Z, Ren J, Stammers DK, Baldwin JE, Harlos K, Schofield CJ (2000) Nat Struct Biol 7:127–133
73. Zhang Z, Ren J, Harlos K, Mckinnon CH, Clifton IJ, Schofield CJ (2002) FEBS Lett 517:7–12
74. Mitchell AJ, Zhu Q, Maggiolo AO, Ananth NR, Hillwig ML, Liu X, Boal AK (2016) Nat Chem Biol 12:636–640
75. Iwata-Reuyl D, Basak A, Townsend CA (1999) J Am Chem Soc 121:11356–11368
76. Borowski T, De Marothy S, Broclawik E, Schofield CJ, Siegbahn PEM (2007) Biochemistry 46:3682–3691
77. Ishikawa N, Tanaka H, Koyama F, Noguchi H, Wang CCC, Hotta K, Watanabe K (2014) Angew Chem Int Ed 53:12880–12884
78. Hollenhorst MA, Bumpus SB, Matthews ML, Bollinger JM, Kelleher NL, Walsh CT (2010) J Am Chem Soc 132:15773–15781
79. Seo MJ, Zhu D, Endo S, Ikeda H, Cane DE (2011) Biochemistry 50:1739–1754
80. Thornburg LD, Lai M-T, Wishnok JS, Stubbe J (1993) Biochemistry 32:14023–14033
81. Bräuer A, Beck P, Hintermann L, Groll M (2016) Angew Chemie Int Ed 55:422–426
82. Meunier B, Bernadou J (2000) Struct Bond 97:1–35

83. Puri M, Company A, Sabenya G, Costas M, Que L (2016) Inorg Chem 55:5818–5827
84. Seo MS, In J-H, Kim SO, Oh NY, Hong J, Kim J, Que L, Nam W (2004) Angew Chem Int Ed 43:2417–2420
85. Steffan N, Grundmann A, Afiyatullov S, Ruan H, Li S-M (2009) Org Biomol Chem 7:4082–4087
86. Kato N, Suzuki H, Takagi H, Uramoto M, Takahashi S, Osada H (2011) ChemBioChem 12:711–714
87. Yan W, Song H, Song F, Guo Y, Wu C-H, Sae Her A, Pu Y, Wang S et al (2015) Nature 527:539–543
88. Peck SC, van der Donk WA (2017) J Biol Inorg Chem. doi:10.1007/s00775-016-1399-y
89. Vaillancourt FH, Yeh E, Vosburg DA, Garneau-Tsodikova S, Walsh CT (2006) Chem Rev 106:3364–3378
90. Blasiak LC, Vaillancourt FH, Walsh CT, Drennan CL (2006) Nature 440:368–371
91. Wong C, Fujimori DG, Walsh CT, Drennan CL (2009) J Am Chem Soc 131:4872–4879
92. Khare D, Wang B, Gu L, Razelun J, Sherman DH, Gerwick WH, Håkansson K, Smith JL (2010) Proc Natl Acad Sci 107:14099–14104
93. Vaillancourt FH, Yin J, Walsh CT (2005) Proc Natl Acad Sci 102:10111–10116
94. Matthews ML, Neumann CS, Miles LA, Grove TL, Booker SJ, Krebs C, Walsh CT, Bollinger JM (2009) Proc Natl Acad Sci 106:17723–17728
95. Srnec M, Wong SD, Matthews ML, Krebs C, Bollinger JM, Solomon EI (2016) J Am Chem Soc 138:5110–5122
96. England J, Guo Y, Farquhar ER, Young VG, Münck E, Que L (2010) J Am Chem Soc 132:8635–8644
97. Srnec M, Wong SD, England J, Que L, Solomon EI (2012) Proc Natl Acad Sci 109:14326–14331
98. Borowski T, Noack H, Radoń M, Zych K, Siegbahn PEM (2010) J Am Chem Soc 132:12887–12898
99. Martinie RJ, Livada J, Chang W, Green MT, Krebs C, Bollinger JM, Silakov A (2015) J Am Chem Soc 137:6912–6919
100. Pavon JA, Fitzpatrick PF (2006) Biochemistry 45:11030–11037
101. Hillas PJ, Fitzpatrick PF (1996) Biochemistry 35:6969–6975
102. Roberts KM, Fitzpatrick PF (2013) IUBMB Life 65:350–357
103. Flydal MI, Martinez A (2013) IUBMB Life 65:341–349
104. Fitzpatrick PF (1999) Annu Rev Biochem 68:355–381
105. Andersen OA, Stokka AJ, Flatmark T, Hough E (2003) J Mol Biol 333:747–757
106. Wang L, Erlandsen H, Haavik J, Knappskog PM, Stevens RC (2002) Biochemistry 41:12569–12574
107. Goodwill KE, Sabatier C, Stevens RC (1998) Biochemistry 37:13437–13445
108. Andersen OA, Flatmark T, Hough E (2002) J Mol Biol 320:1095–1108
109. Kemsley JN, Mitić N, Zaleski KL, Caradonna JP, Solomon EI (1999) J Am Chem Soc 121:1528–1536
110. Wasinger EC, Mitić N, Hedman B, Caradonna J, Solomon EI, Hodgson KO (2002) Biochemistry 41:6211–6217
111. Chow MS, Eser BE, Wilson SA, Hodgson KO, Hedman B, Fitzpatrick PF, Solomon EI (2009) J Am Chem Soc 131:7685–7698
112. Krzyaniak MD, Eser BE, Ellis HR, Fitzpatrick PF, McCracken J (2013) Biochemistry 52:8430–8441
113. Roberts KM, Pavon JA, Fitzpatrick PF (2013) Biochemistry 52:1062–1073
114. Pavon JA, Eser B, Huynh MT, Fitzpatrick PF (2010) Biochemistry 49:7563–7571
115. Massey V (1994) J Biol Chem 269:22459–22462
116. Pavon JA, Fitzpatrick PF (2009) J Am Chem Soc 131:4582–4583
117. Moran GR, Derecskei-Kovacs A, Hillas PJ, Fitzatrick PF (2000) J Am Chem Soc 122:4535–4541
118. Panay AJ, Fitzpatrick PF (2010) J Am Chem Soc 132:5584–5585
119. Pavon JA, Fitzpatrick PF (2005) J Am Chem Soc 127:16414–16415
120. Frantom PA, Pongdee R, Sulikowski GA, Fitzpatrick PF (2002) J Am Chem Soc 124:4202–4203
121. Feng Y, Ke C-Y, Xue G, Que L (2009) Chem Commun 1:50–52
122. Daughtry KD, Xiao Y, Stoner-Ma D, Cho E, Orville AM, Liu P, Allen KN (2012) J Am Chem Soc 134:2823–2834
123. Wang XZ, Li B, Herman PL, Weeks DP (1997) Appl Environ Microbiol 63:1623–1626
124. Martins BM, Svetlitchnaia T, Dobbek H (2005) Structure 13:817–824
125. Capyk JK, D'Angelo I, Strynadka NC, Eltis LD (2009) J Biol Chem 284:9937–9946
126. Lee J, Simurdiak M, Zhao H (2005) J Biol Chem 280:36719–36728
127. Sydor PK, Barry SM, Odulate OM, Barona-Gomez F, Haynes SW, Corre C, Song L, Challis GL (2011) Nat Chem 3:388–392
128. Kauppi B, Lee K, Carredano E, Parales RE, Gibson DT, Eklund H, Ramaswamy S (1998) Structure 6:571–586
129. Ashikawa Y, Fujimoto Z, Noguchi H, Habe H, Omori T, Yamane H, Nojiri H (2006) Structure 14:1779–1789
130. D'Ordine RL, Rydel TJ, Storek MJ, Sturman EJ, Moshiri F, Bartlett RK, Brown GR, Eilers RJ, Dart C, Qi Y, Flasinski S, Franklin SJ (2009) J Mol Biol 392:481–497
131. Penfield JS, Worrall LJ, Strynadka NC, Eltis LD (2014) J Biol Chem 289:25523–25536
132. Dumitru R, Jiang WZ, Weeks DP, Wilson MA (2009) J Mol Biol 392:498–510
133. Parales RE, Parales JV, Gibson DT (1999) J Bacteriol 181:1831–1837
134. Wolfe MD, Parales JV, Gibson DT, Lipscomb JD (2001) J Biol Chem 276:1945–1953
135. Wolfe MD, Altier DJ, Stubna A, Popescu CV, Münck E, Lipscomb JD (2002) Biochemistry 41:9611–9626
136. Wolfe MD, Lipscomb JD (2003) J Biol Chem 278:829–835
137. Chakrabarty S, Austin RN, Deng D, Groves JT, Lipscomb JD (2007) J Am Chem Soc 129:3514–3515
138. Wackett LP, Kwart LD, Gibson DT (1988) Biochemistry 27:1360–1367
139. Rivard BS, Rogers MS, Marell DJ, Neibergall MB, Chakrabarty S, Cramer CJ, Lipscomb JD (2015) Biochemistry 54:4652–4664
140. Tiago de Oliveira F, Chanda A, Banerjee D, Shan X, Mondal S, Que L, Bominaar EL, Münck E, Collins TJ (2007) Science 315:835–838
141. Ghosh M, Singh KK, Panda C, Weitz A, Hendrich MP, Collins TJ, Dhar BB, Gupta SS (2014) J Am Chem Soc 136:9524–9527
142. Mills MR, Weitz AC, Hendrich MP, Ryabov AD, Collins TJ (2016) J Am Chem Soc 138:13866–13869
143. Van Heuvelen KM, Fiedler AT, Shan X, De Hont RF, Meier KK, Bominaar EL, Münck E, Que L (2012) Proc Natl Acad Sci 109:11933–11938
144. Chen K, Que L (2001) J Am Chem Soc 123:6327–6337
145. Chen K, Costas M, Kim J, Tipton AK, Que L (2002) J Am Chem Soc 124:3026–3035
146. Chow TWS, Wong ELM, Guo Z, Liu Y, Huang JS, Che CM (2010) J Am Chem Soc 132:13229–13239
147. Prat I, Mathieson JS, Güell M, Ribas X, Luis JM, Cronin L, Costas M (2011) Nat Chem 3:788–793
148. Hitomi Y, Arakawa K, Funabiki T, Kodera M (2012) Angew Chem Int Ed 51:3448–3452

149. Oloo WN, Que L (2015) Acc Chem Res 48:2612–2621
150. Lyakin OY, Zima AM, Samsonenko DG, Bryliakov KP, Talsi EP (2015) ACS Catal 5:2702–2707
151. Serrano-Plana J, Oloo WN, Acosta-Rueda L, Meier KK, Verdejo B, García-España E, Basallote MG, Münck E, Que L, Company A, Costas M (2015) J Am Chem Soc 137:15833–15842
152. Baldwin JE, Bradley M (1990) Chem Rev 90:1079–1088
153. Roach PL, Clifton IJ, Hensgens CMH, Shibata N, Schofield CJ, Hajdu J, Baldwin JE (1997) Nature 387:827–830
154. Baldwin JE, Abraham SE (1988) Nat Prod Rep 5:129–145
155. Burzlaff NI, Rutledge PJ, Clifton IJ, Hensgens CMH, Pickford M, Adlington RM, Roach PL, Baldwin JE (1999) Nature 401:721–724
156. Bukowski MR, Koehntop KD, Stubna A, Bominaar EL, Halfen JA, Münck E, Nam W, Que L (2005) Science 310:1000–1002
157. Lundberg M, Siegbahn PEM, Morokuma K (2008) Biochemistry 47:1031–1042
158. Lundberg M, Kawatsu T, Vreven T, Frisch MJ, Morokuma K (2009) J Chem Theory Comput 5:222–234
159. Brown-Marshall CD, Diebold AR, Solomon EI (2010) Biochemistry 49:1176–1182
160. Bleecker AB, Kende H (2000) Annu Rev Cell Dev Biol 16:1–18
161. Wang KLC, Li H, Ecker JR (2002) Plant Cell 14:S131–S151
162. Dilley DR, Wang Z, Kadirjan-Kalbach DK, Ververidis F, Beaudry R, Padmanabhan K (2013) AoB Plants 5:1–23
163. Goto M, Hyodo H (1987) Plant Cell Physiol 28:405–414
164. Xiong W, Morgan JA, Ungerer J, Wang B, Maness P-C, Yu J (2015) Nat Plants 1:15053
165. Zhu T, Xie X, Li Z, Tan X, Lu X (2015) Green Chem 17:421–434
166. Lynch S, Eckert C, Yu J, Gill R, Maness P-C (2016) Biotechnol Biofuels 9:3
167. Zavřel T, Knoop H, Steuer R, Jones PR, Červený J, Trtílek M (2016) Bioresour Technol 202:142–151
168. Dong JG, Fernández-Maculet JC, Yang SF (1992) Proc Natl Acad Sci USA 89:9789–9793
169. Zhang Z, Ren J-S, Clifton IJ, Schofield CJ (2004) Chem Biol 11:1383–1394
170. Zhou J, Rocklin AM, Lipscomb JD, Que L Jr, Solomon EI (2002) J Am Chem Soc 124:4602–4609
171. Zhang Z, Schofield CJ, Baldwin JE, Thomas P, John P (1995) Biochem J 307:77–85
172. McGarvey DJ, Christoffersen RE (1992) J Biol Chem 267:5964–5967
173. Ververidis P, John P (1991) Phytochemistry 30:725–727
174. Fernandez-Maculet JC, Dong JG, Yang SF (1993) Biochem Biophys Res Commun 193:1168–1173
175. Rocklin AM, Tierney DL, Kofman V, Brunhuber NMW, Hoffman BM, Christoffersen RE, Reich NO, Lipscomb JD, Que L (1999) Proc Natl Acad Sci 96:7905–7909
176. Tierney DL, Rocklin AM, Lipscomb JD, Que L, Hoffman BM (2005) J Am Chem Soc 127:7005–7013
177. Arciero DM, Lipscomb JD, Huynh BH, Kent TA, Münck E (1983) J Biol Chem 258:14981–14991
178. Arciero DM, Lipscomb JD (1986) J Biol Chem 261:2170–2178
179. Chen VJ, Orville AM, Harpel MR, Frolik CA, Surerus KK, Münck E, Lipscomb JD (1989) J Biol Chem 264:21677–21681
180. Yang TC, Wolfe MD, Neibergall MB, Mekmouche Y, Lipscomb JD, Hoffman BM (2003) J Am Chem Soc 125:7056–7066
181. Lipscomb JD (2014) J Biol Chem 289:15141–15153
182. Fielding AJ, Lipscomb JD, Que L (2014) J Biol Inorg Chem 19:491–504
183. Rocklin AM, Kato K, Liu H, Que L, Lipscomb JD (2004) J Biol Inorg Chem 9:171–182
184. Thrower J, Mirica LM, McCusker KP, Klinman JP (2006) Biochemistry 45:13108–13117
185. Mirica LM, Klinman JP (2008) Proc Natl Acad Sci 105:1814–1819
186. Mirica LM, Mccusker KP, Munos JW, Liu H, Klinman JP (2008) J Am Chem Soc 130:8122–8123
187. Kovaleva EG, Lipscomb JD (2007) Science 316:453–457
188. Mbughuni MM, Chakrabarti M, Hayden JA, Bominaar EL, Hendrich MP, Münck E, Lipscomb JD (2010) Proc Natl Acad Sci 107:16788–16793
189. Johansson N, Persson K, Larsson C, Norbeck J (2014) BMC Biochem 15:22
190. Martinez S, Hausinger RP (2016) Biochemistry 55:5989–5999
191. Fukuda H, Ogawa T, Tazaki M, Nagahama K, Fujii T, Tanase S, Morino Y (1992) Biochem Biophys Res Commun 188:483–489
192. Nagahama K, Ogawa T, Fujii T, Tazaki M, Goto M, Fukuda H (1991) J Gen Microbiol 137:1641–1646
193. Liu P, Murakami K, Seki T, He X, Yeung S, Kuzuyama T, Seto H, Liu H (2001) J Am Chem Soc 123:4619–4620
194. Hammerschmidt F (1991) J Chem Soc Perkin Trans 1:1993–1996
195. Liu P, Liu A, Yan F, Wolfe MD, Lipscomb JD, Liu H (2003) Biochemistry 42:11577–11586
196. Hammerschmidt F, Bovermannb G, Karl B (1990) Liebigs Ann Chem 1055–1061
197. Wang C, Chang W, Guo Y, Huang H, Peck SC, Pandelia ME, Lin G, Liu H, Krebs C, Bollinger JM (2013) Science 342:991–995
198. Chang WC, Dey M, Liu P, Mansoorabadi SO, Moon SJ, Zhao ZK, Drennan CL, Liu HW (2013) Nature 496:114–118
199. Chang W, Mansoorabadi SO, Liu H (2013) J Am Chem Soc 135:8153–8156
200. Yun D, Dey M, Higgins LJ, Yan F, Liu H, Drennan CL (2011) J Am Chem Soc 133:11262–11269
201. Wang Y, Li J, Liu A (2017) J Biol Inorg Chem. doi:10.1007/s00775-017-1436-5